

Energy-Efficient URLLC Service Provision via a Near-Space Information Network

Puguang An, Xianbin Cao, *Senior Member, IEEE*, Peng Yang, *Member, IEEE*, Kun Guo, *Member, IEEE*, Yue Gao, *Senior Member, IEEE*, and Tony Q. S. Quek, *Fellow, IEEE*

Abstract

The integration of a near-space information network (NSIN) with the reconfigurable intelligent surface (RIS) is envisioned to significantly enhance the communication performance of future wireless communication systems by proactively altering wireless channels. This paper investigates the problem of deploying a RIS-integrated NSIN to provide energy-efficient, ultra-reliable and low-latency communications (URLLC) services. We mathematically formulate this problem as a resource optimization problem, aiming to maximize the effective throughput and minimize the system power consumption, subject to URLLC and physical resource constraints. The formulated problem is challenging in terms of accurate channel estimation, RIS phase alignment, and effective solution design. We propose a joint resource allocation algorithm to handle these challenges. In this algorithm, we develop an accurate channel estimation approach by exploring message passing and optimize phase shifts of RIS reflecting elements to further increase the channel gain. Besides, we derive an analysis-friendly expression of decoding error probability and decompose the problem into two-layered optimization problems by analyzing the monotonicity, which makes the formulated problem analytically tractable. Extensive simulations have been conducted to verify the performance of the proposed algorithm. Simulation results show that the proposed algorithm can achieve outstanding channel estimation performance and is more energy-efficient than diverse benchmark algorithms.

Index Terms

Near-space information network, reconfigurable intelligent surface, electromagnetic channel estimation, URLLC, energy efficiency

I. INTRODUCTION

The upcoming sixth generation (6G) communication systems have the unprecedented requirements for ultra-reliability, ultra-low latency, and extremely high data rates that the fifth generation (5G) communication systems

P. An is with the School of Electronic and Information Engineering, Beihang University, Beijing 100191, China. X. Cao and P. Yang are with the School of Electronic and Information Engineering, Beihang University, Beijing 100191, China, also with the Key Laboratory of Advanced Technology of Near Space Information System (Beihang University), Ministry of Industry and Information Technology of China, Beijing 100191, China, and also with the Peng Cheng Laboratory, Department of Mathematics and Theories, Shenzhen, Guangdong 518055, China. K. Guo is with the School of Communication and Electronic Engineering, East China Normal University, Shanghai 200062, China. Y. Gao is with the School of Computer Science, Fudan University, Shanghai 200433, China. T. Q. S. Quek is with the Information Systems Technology and Design, Singapore University of Technology and Design, 487372 Singapore.

cannot well fulfill [1]. Ultra-reliable and low-latency communications (URLLC), which is one of the three pillar services for the 5G systems, will still act as a pillar service for the 6G systems. URLLC can empower diverse mission-critical applications including intelligent transportation systems, autonomous driving, telemedicine, industrial automation, Tactile Internet, real-time control in Digital Twins, and Metaverse.

It's widely considered that space-air-ground integrated communication systems are a crucial system architecture that can satisfy the unprecedented requirements of 6G systems. A near-space information network (NSIN), composed of various near-space platforms (e.g., airships), medium/low-altitude platforms (e.g., medium/low-altitude unmanned aerial vehicles (UAVs)), is a network system that can acquire, transmit, and process space electromagnetic (EM) signals in real-time. It's the core component of the space-air-ground integrated communication systems. Compared to space-based networks, NSIN is much closer to terrestrial users and can provide high-capacity communication services. Compared with terrestrial networks, NSIN can quickly extend the communication distance and is robust to unexpected events (e.g., diverse natural disasters). Thus, NSIN can provide wide-area and reliable communication coverage. In this regard, NSIN integrates the advantages of space-based networks and terrestrial networks and becomes an important supplement to terrestrial networks and space-based networks. It's envisioned that resorting to NSIN will become a new regime for enabling URLLC [2], [3]. The authors of this manuscript have also demonstrated the feasibility of delivering reliable and low-latency control-and-non-payload EM signals using one of our manufactured near-space airships during the execution of many projects on airship-supported intelligent transportation systems and meteorological observations over the past few years [4].

Except for the mentioned space-air-ground integrated systems, reconfigurable intelligent surface (RIS) has emerged as a promising paradigm to achieve smart wireless reflection channels for 6G systems. RIS is a planar surface consisting of many passive reflecting elements for EM waves, each of which can separately change the amplitude and/or phase of impinging EM signals. With the deployment of RIS, wireless channels between transmitters and receivers can be flexibly reconfigured to achieve desired realizations and distributions. Thus, RIS provides a new paradigm to fundamentally address the complex EM signal interference and channel fading issues and potentially achieves a significant improvement in terms of throughput and reliability of wireless communication systems [5].

Different from existing advanced communication techniques (e.g., beamforming, dynamic rate control) to realize ultra-reliable and high-capacity transmission by adapting to channel conditions, both NSIN and RIS can proactively alter the wireless channels to significantly improve communication performance. Specifically, NSIN can achieve rich line-of-sight (LoS) transmission through trajectory/location control. RIS can create desired LoS links for EM wave propagation and eliminate EM signal interference via smart EM signal reflection.

The integration of NSIN with RIS achieves complementary advantages, which will significantly increase the design flexibility of NSIN, reduce cost, and improve transmission performance. Through mounting RIS on an airborne platform of NSIN, RIS can achieve a 360° panoramic full-angle reflection toward target nodes. By deploying RIS-integrated NSIN, wide-area interference inherent in NSIN can be mitigated, and the spectral efficiency of NSIN can be improved. Meanwhile, the integration of RIS in NSIN will improve the energy efficiency of NSIN due to the low hardware and energy costs of RIS. Related work and motivations and contributions are two sections

A. State of the Art

Recently, research on the URLLC-enabled UAV network or NSIN has attracted much attention, as outlined in [3], [6]–[15]. For example, the work in [3] proposed an NSIN with low/medium/high altitude platforms to support URLLC applications. The authors developed a complex network optimization tool, i.e., polychromatic sets, to analyze the performance of each link. Based on the analysis results, they designed distributed and centralized link selection schemes to select end-to-end links that could meet the stringent latency and reliability requirements of URLLC. The work in [6] utilized a UAV relay to send short URLLC control packets from a controller to many mobile robots. In particular, the authors investigated the optimization problem in terms of UAV deployment, beamwidth, transmit power, and blocklength allocated to each robot and proposed an iterative search method to obtain the optimal solution. The work in [7] investigated the optimization problem of UAV deployment altitude, blocklength, transmission power, and update generation rate to ensure that the ground destination node can acquire information timely in an URLLC-enabled UAV network. The work in [8] analyzed channel quality indicator (CQI) aging effects in URLLC under the finite blocklength regime and utilized a Recurrent Neural Network (RNN) approach to predict the next CQI for UAV control information exchange. The authors in [9] studied the failed packet reception probability and effective throughput of URLLC control links in UAV communications. They derived the closed-form expression of packet error probability and throughput using Gaussian-Chebyshev quadrature and obtained the optimal packet length using an exhaustive search. Besides, based on the observation of the high possibility of establishing LoS links between UAVs and ground users, the authors in [10] investigated the potential of using UAVs in supporting URLLC. They characterized the transmission latency, reliability, and network availability of UAV networks, optimized the UAV deployment altitude, and allocated bandwidth that minimized the required total bandwidth for URLLC.

RIS is an important emerging technique that can provide optimized energy and spectral efficiency for communication systems. Recent studies showed that a RIS-assisted communication system could be 40% more energy-efficient than a relay-assisted system [16]. Above works [3], [6]–[13] did not investigate the NSIN- or UAV-assisted URLLC systems with the aid of RIS. Nonetheless, the integration of RIS in aerial URLLC communication systems has recently attracted extensive attention in the research community [17]–[20]. For instance, the authors in [17] proposed a UAV-RIS system to support the stringent URLLC constraints and formulated an optimization framework in terms of UAVs' locations, the phase shift of RIS, and the blocklength of URLLC. To solve the formulated problem, a deep neural network (DNN) architecture was designed to obtain 3-D deployment locations of UAVs, and an iterative optimization scheme was explored to optimize the phase shift and blocklength. The work in [18] considered a scenario of deploying a UAV and a ground RIS to deliver URLLC packets between ground Internet-of-Things (IoT) devices. The authors proposed to jointly optimize the passive beamforming, the deployment location of a UAV, and the blocklength to minimize the packet decoding error probability (DEP). A computationally efficient Nelder–Mead simplex approach was utilized to solve the joint optimization problem. The authors in [19] developed a joint passive beamforming and UAV trajectory optimization approach to support URLLC applications over UAV/RIS-based systems. They first built UAV/RIS-based channel models in a finite blocklength regime. Then, they formulated a finite-blocklength coding-based energy-efficiency maximization problem. Next, an alternative optimization scheme

was utilized to optimize UAV transmit power, passive beamforming, and UAV trajectory alternatively. Additionally, the authors in [20] investigated the benefits of UAV/RIS-based systems to passively relay low-latency information sampled by Internet of Things (IoT) devices to a base station (BS). For this aim, they formulated a joint optimization problem of UAV altitude, the phase shift of RIS, and communication scheduling, aiming to minimize the expected sum Age-of-Information (AoI) under a reliable decoding constraint. They also designed a DRL framework based on proximal policy optimization to solve the optimization problem.

B. Motivations and Contributions

Although the issue of designing UAV/RIS-based systems to support URLLC applications was investigated in the works [17]–[20], they did not consider the scenario of integrating high altitude platforms (HAPs), UAVs, and aerial RIS to provide wide-area and robust communication coverage in an energy- and cost-efficient manner. Most recently, the works in [21], [22] investigated the integration of NSIN and RIS. For example, the authors in [21] considered a novel wireless architecture composed of a RIS-enabled HAP and multiple UAVs. The HAP-RIS could overcome the limitations of conventional terrestrial RIS and achieve rich LoS and full-area coverage. The UAVs that would receive backhaul reflection signals from HAP-RIS were deployed to serve terrestrial flash crowd traffic. They formulated and solved a joint optimization problem of HAP deployment location and phase shift of RIS to increase the energy efficiency of UAVs. The work in [22] considered a scenario of deploying a UAV-RIS to assist the HAP downlink transmission. The authors formulated an optimization problem of maximizing the signal-to-noise ratio (SNR) of ground users by jointly optimizing the UAV trajectory and the phase shift of UAV-RIS. They developed a model-free reinforcement learning framework to learn the UAV trajectory and adjust the phase shift according to the learned UAV trajectory.

The works [21], [22], however, investigated the high throughput scenario instead of the URLLC scenario. Moreover, they did not study the crucial HAP-UAV channel estimation problem. A LoS propagation assumption between a HAP and a low-altitude UAV was enforced in [21], [22]. This assumption will be unreasonable as the received signals by a low-altitude UAV include both LoS and non-line-of-sight (NLoS) (e.g., reflected/scattered signals) components. Therefore, it's essential to study the HAP-UAV channel estimation issue.

To tackle the above issues, this paper proposes to design a RIS-integrated NSIN to support energy-efficient URLLC services, which leverages the advantages of power control and RIS. The main contributions of this paper are summarized as follows:

- We formulate the problem of providing energy-efficient URLLC services using a RIS-integrated NSIN as a resource optimization problem. The goal of this problem is to maximize the effective throughput and minimize the system power consumption, subject to URLLC and physical resource constraints. The formulated problem is challenging in terms of channel estimation, RIS phase shift optimization, theoretical analysis, and effective solution.
- To handle these challenges, we propose a joint resource allocation algorithm in which we first develop a probabilistic channel model to capture the sparsity of the HAP-UAV channel and then design a novel channel estimation approach by message passing to accurately estimate the HAP-UAV channel.

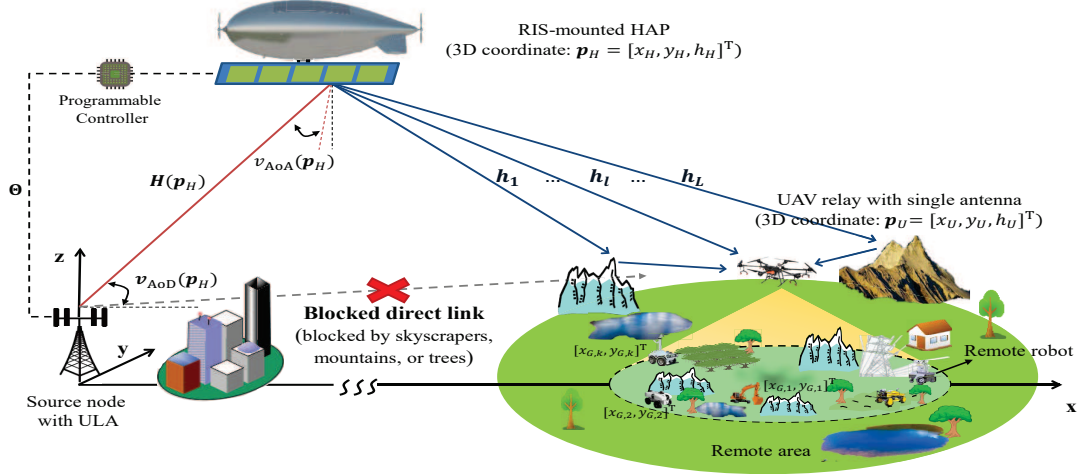


Fig. 1. A downlink URLLC transmission scenario with a RIS-integrated NSIN communication system.

- Second, we apply a maximum-ratio transmission (MRT) strategy to maximize the signal-to-noise ratio (SNR) and design a RIS phase shift optimization strategy, resulting in a suboptimal HAP-UAV channel gain. Besides, we derive an analysis-friendly expression of DEP by Taylor expansion to make the formulated problem analytically tractable and help to lower the DEP value.
- Third, through analyzing the monotonicity of the objective function in the feasible region, we decouple the decision variables and horizontally decompose the problem into a BS-Layer optimization problem and a UAV-Layer optimization problem. An iterative optimization strategy is then explored to optimize transmit power and blocklength alternately.
- Finally, the proposed algorithm is compared with diverse benchmarks to verify its performance, and the impact of various design parameters is comprehensively discussed through extensive simulations. Simulation results show that the proposed algorithm can achieve accurate HAP-UAV channel estimation and can provide energy-efficient URLLC services.

II. SYSTEM MODEL AND PROBLEM FORMULATION

A. System Model

We consider a downlink transmission scenario based on a RIS-integrated NSIN communication system for energy-efficient URLLC service provision. As illustrated in Fig. 1, the system mainly includes a base station (BS), a RIS-mounted HAP, a low-altitude UAV, and multiple ground remote URLLC robots. The BS is designated to transmit ultra-reliable and low-latency signals towards these remote robots for accomplishing some critical tasks (e.g., grid, pipeline, security, and remote railway patrol, farming, and mining). A direct propagation path between the BS and a remote URLLC robot, however, will be blocked by numerous physical obstructions on the ground (e.g., skyscrapers, mountains, and trees) over the remote propagation path. Then, the RIS-mounted HAP and the UAV can work cooperatively to establish ultra-reliable near-space communication links between the BS and multiple

remote URLLC robots. The RIS-mounted HAP acts as a passive flying relay, and the UAV acts as an active flying relay. In this system, the BS is located at the origin and equipped with a uniform linear-array (ULA) antenna with M antenna array elements. The antenna gain equals G , and the spacing of adjacent antenna elements is d_{BS} . There are K URLLC robots with a single antenna configuration, and they are randomly and uniformly distributed in a considered area \mathcal{G} . The URLLC robot set is denoted as $\mathcal{K} = \{1, \dots, K\}$, and denote the coordinate of the k -th robot by $\mathbf{p}_G = [x_{G,k}, y_{G,k}]^T$. The UAV is equipped with an omnidirectional antenna, hovering in the air with a fixed three-dimensional (3-D) coordinate $\mathbf{p}_U = [x_U, y_U, h_U]^T$. A decoding-and-forward (DF) relay strategy is adopted to flexibly control the blocklength for the BS-HAP-UAV link and the UAV-to-ground (UtG) link. Moreover, the frequency division multiple access (FDMA) manner is exploited to eliminate intra-cell interference.

For the RIS-mounted HAP, we assume that a ULA-structured RIS is deployed directly below the HAP to provide wide-area and full-angle coverage. The RIS includes N passive reflecting elements, separated by the spacing d_{RIS} . We assume that the BS array is deployed on the origin. The HAP hovers at a fixed point $\mathbf{p}_H = [x_H, y_H, h_H]^T$ in the stratosphere. We assume that all elements of the RIS are turned on without power amplification. Thus, the diagonal phase shift matrix of the RIS can be modeled as [23]–[25]

$$\Theta = \text{diag} \{e^{j\theta_1}, e^{j\theta_2}, \dots, e^{j\theta_N}\} \in \mathbb{C}^{N \times N} \quad (1)$$

where $\theta_n \in (0, 2\pi]$ is the phase shift parameter of the n -th element. During the first transmission phase, the BS will transmit URLLC signals to the UAV with the assistance of the HAP relay. In this phase, a cascading channel comprised of the BS-HAP channel and the HAP-UAV channel is constructed. Denote the BS-HAP channel by $\mathbf{H} \in \mathbb{C}^{N \times M}$, and the HAP-UAV channel by $\mathbf{h} \in \mathbb{C}^N$. Therefore, the received signal at the UAV from the BS can be expressed as

$$y = \sqrt{P_b G} \mathbf{h}^H \Theta \mathbf{H} \mathbf{v} u_1 + n \quad (2)$$

where P_b is the source transmit power of BS, $\mathbf{v} \in \mathbb{C}^{N \times 1}$ is the unit-magnitude precoding vector, u_1 is the transmission signal with unit-power. n is the additive white Gaussian noise (AWGN) vector, following a distribution of $\mathcal{CN}(0, \sigma_0^2)$, and σ_0^2 is the noise power. Then, the instantaneous signal-to-noise ratio (SNR) experienced by the UAV, denoted by SNR_u , can be given by

$$SNR_u = P_b G |\mathbf{h}^H \Theta \mathbf{H} \mathbf{v}|^2 / \sigma_0^2 \quad (3)$$

In the second transmission phase, the UAV decodes received URLLC packets from the BS and re-encodes and forwards the packets to robots via the FDMA scheme. Denote the UtG channel by $\{g_k\}$, $\forall k \in \mathcal{K}$. Then the received signal of any robot in the considered area can be expressed as

$$y_k = \sqrt{P_u} g_k u_2 + n_k \quad (4)$$

where P_u is the transmit power of UAV, u_2 is the transmission signal with unit-power, the noise n_k is subject to a normal distribution with zero mean and variance σ_k^2 . Then, the instantaneous SNR experienced by robot k , denoted by SNR_k , can be given by

$$SNR_k = P_u |g_k|^2 / \sigma_k^2 \quad (5)$$

B. BS-HAP Channel Model

In practice, HAP is usually deployed in an EM propagation environment without rich scatters. It's then reasonable to assume that the BS-HAP channel is dominated by the LOS component. The resulting BS-HAP channel matrix can be expressed as

$$\mathbf{H} = \alpha \mathbf{a}_{\text{RIS}}(v_{\text{AoD}}(\mathbf{p}_H)) \mathbf{a}_{\text{BS}}^H(v_{\text{AoA}}(\mathbf{p}_H)) \quad (6)$$

where α represents the complex channel gain, capturing path loss and additional attenuation caused by the EM propagation environment (e.g., rain and water vapor). $\mathbf{a}_{\text{RIS}}(\cdot) \in \mathbb{C}^M$, $\mathbf{a}_{\text{BS}}(\cdot) \in \mathbb{C}^N$ are the array steering vectors of BS and RIS-mounted HAP, respectively, with

$$\mathbf{a}_{\text{RIS}}(\cdot) = [1, e^{-j2\pi\bar{d}_{\text{RIS}}\sin(\cdot)}, \dots, e^{-j2\pi(M-1)\bar{d}_{\text{RIS}}\sin(\cdot)}]^T \quad (7)$$

$$\mathbf{a}_{\text{BS}}(\cdot) = [1, e^{-j2\pi\bar{d}_{\text{BS}}\sin(\cdot)}, \dots, e^{-j2\pi(N-1)\bar{d}_{\text{BS}}\sin(\cdot)}]^T \quad (8)$$

where $\bar{d}_{\text{RIS}} = d_{\text{RIS}}/\lambda$, $\bar{d}_{\text{BS}} = d_{\text{BS}}/\lambda$, λ is wavelength. $v_{\text{AoD}}(\mathbf{p}_H)$ and $v_{\text{AoA}}(\mathbf{p}_H)$ are the AoD and AoA of the BS-HAP link, respectively. Aided by precise position information obtained by GPS or other positioning systems, both AoA and AoD can be obtained.

Owing to the relative stability of the BS-HAP channel, we assume that its channel gain can be maintained stable for a long time and continuous estimation is not necessary. Therefore, the channel gain is considered to be known in advance in this paper.

C. HAP-UAV Channel Model

Unlike the BS-HAP channel, the EM propagation environment of the HAP-UAV channel will be more complex. A UAV is usually deployed close to robots to establish high-quality UtG links; as a result, there is limited physical scatters (e.g., trees and mountains) around the UAV, as shown in Fig. 1. We consider such a case that the HAP-UAV channel fading consists of large-scale channel fading and small-scale channel fading caused by limited reflected/scattered paths. The large-scale fading can be obtained by computing free-space path loss and meteorological loss. Nevertheless, it is highly challenging to compute the small-scale fading; as a result, we need to estimate it. In addition, due to the high-frequency transmission characteristic [26], the transmitted signal has a sound geometric characteristic. To this end, we adopt a narrowband geometric block-fading channel model in [27]

$$\mathbf{h} = \sum_{l=1}^L \beta_l \mathbf{a}_{\text{RIS}}(\omega_l) \quad (9)$$

where β_l and ω_l represent the complex path gain and AoD of the l -th path, respectively.

D. Decoding Error Probability in a URLLC Regime

Different from conventional wireless communications, a URLLC regime has stringent QoS requirements on transmission latency and reliability (e.g., DEP). To satisfy these requirements, the blocklength of URLLC packets should be controlled within a finite length. However, the Shannon's capacity formula fails to build the relationship between these performance metrics and the blocklength. Shannon's capacity refers to the maximum achievable

channel coding rate (MAR) that can be obtained with arbitrary transmission latency, which indicates that a signal blocklength should be sufficiently long. To tackle this issue, we leverage tight MAR approximations [28], [29] of the BS-HAP-UAV link (denoted by R_u) and the UAV-GU link (denoted by R_k), which are extremely precise under the assumption that a blocklength is greater than 50 symbols, i.e.,

$$R_* = \log_2(1 + SNR_*) - \sqrt{\frac{1 - (1 + SNR_*)^{-2}}{b_*}} \frac{Q^{-1}(\varepsilon_*)}{\ln 2} \quad (10)$$

where $* \in \{u, k\}$, $Q(x) = \frac{1}{\sqrt{2\pi}} \int_x^\infty \exp(-t^2/2) dt$ is a Gaussian Q-function, which is also a monotonically decreasing function of the argument. b_u and b_k are the blocklengths allocated to the BS-HAP-UAV link and the UAV-GU link, respectively. As the UAV adopts the DF strategy, the BS-HAP-UAV link and the UAV-GU link can be configured with different blocklengths. ε_u and $\{\varepsilon_k\}_{k=1}^K$ are the DEPs of the UAV and the robots, respectively. F_k is denoted as the size of a URLLC packet transmitted to the k -th robot from the UAV, and F_B the size of a URLLC packet sent by the BS. According to the FDMA downlink transmission scheme, we have $R_u = F_B/b_u$ and $R_k = F_k/b_k$ [30]–[33]. The corresponding DEP is then given by

$$\varepsilon_* = Q\left(\sqrt{\frac{b_*}{1 - (1 + SNR_*)^{-2}}} (\log_2(1 + SNR_*) - R_*) \ln 2\right) \triangleq Q(f(b_*, SNR_*)) \quad (11)$$

E. Problem Formulation

Based on the above system model, this subsection aims to formulate a joint transmission power, blocklength, and RIS phase shift optimization problem for providing energy-efficient URLLC services for robots.

1) *URLLC and physical resource constraints*: DEP and communication latency are crucial performance metrics of URLLC services, which should be carefully dealt with. Let ε_u represent the DEP at the UAV, and ε_k the DEP at k -th robot. As decoding errors, either at the UAV or at a GU, will result in transmission failure, the overall DEP experienced by the k -th robot can be written as

$$\varepsilon = (1 - \varepsilon_u)\varepsilon_k + \varepsilon_u = \varepsilon_k + \varepsilon_u - \varepsilon_u\varepsilon_k < \varepsilon_k + \varepsilon_u \quad (12)$$

Note that we omit the term $\varepsilon_u\varepsilon_k$ as it's much smaller than the other two terms. From (12), we can observe that reducing the overall DEPs is equivalent to reducing the DEPs of UAV and robots, respectively. What's more, as a backbone link, it's significant to provide an extremely low and stable DEP over the BS-HAP-UAV link under any circumstances. The statistical feature of the cascaded BS-HAP-UAV channel and the UtG channel is also quite different. The cascaded BS-HAP-UAV channel is deterministic. The UtG channel is random, and then an expected constraint on the DEP of a robot should be enforced. Hence, we separately impose the DEP constraints of the UAV and robots as follows,

$$\varepsilon_u \leq \varepsilon_u^{\text{th}} \quad (13)$$

$$\mathbb{E}[\varepsilon_k] \leq \varepsilon_k^{\text{th}}, \forall k \in \mathcal{K} \quad (14)$$

where $\varepsilon_u^{\text{th}}$ and $\varepsilon_k^{\text{th}}$ are the tolerable DEPs of the UAV and the k -th GU, respectively, $\mathbb{E}[\cdot]$ the expectation operator.

Next, we discuss the communication latency-related constraint. To guarantee the ultra-low latency performance, the blocklength should be maintained at a finite length [17], [30], [31]. Note that the UAV adopts the FDMA-DF

mode, which allows us to flexibly design different blocklengths over each communication link to further boost the overall NSIN system performance. Define the minimum and maximum blocklength sets allocated to the BS and the UAV as $\{B_u^{\min}, B_u^{\max}\}$ and $\{B^{\min}, B^{\max}\}$, respectively. Thus, the latency-related constraints can be described as [30], [31]

$$B_u^{\min} \leq b_u \leq B_u^{\max}, b_u \in \mathbb{Z}^+ \quad (15)$$

$$B^{\min} \leq b_k \leq B^{\max}, b_k \in \mathbb{Z}^+, \forall k \in \mathcal{K} \quad (16)$$

Finally, we discuss the constraints on BS and UAV transmit power. We investigate the power control problem of BS and UAV to achieve energy-efficient URLLC packet transmission. The configured transmit power is not allowed to exceed a power budget. Denote the maximum transmit power of the BS and the UAV by P_B and P_U , respectively. Therefore, we have the following transmit power constraints

$$0 < P_b \leq P_B \quad (17)$$

$$0 < P_u \leq P_U \quad (18)$$

2) *Objective function design:* Energy efficiency is a key performance evaluation indicator for UAV-assisted cellular networks [34]–[36]. Based on the concepts of MAR, and BS and UAV transmit power, we design an energy efficiency model to represent the objective function. The energy efficiency model is defined as the ratio of the effective throughput [30] to the system power consumption, which is given by

$$\eta_k = \frac{R_u(1 - \varepsilon_u/\varepsilon_u^{\text{th}}) + R_k(1 - \varepsilon_k/\varepsilon_k^{\text{th}})}{P_b/P_B + P_u/P_U}, \forall k \in \mathcal{K} \quad (19)$$

where the system power consumption denotes the sum of normalized BS and UAV transmit power.

Remark 1: The value of DEP is usually extremely small, resulting in correct decoding probabilities $1 - \varepsilon_u$ and $1 - \varepsilon_k$ approximately equals 1. In this case, we must scale up the DEP value by multiplying it by $\frac{1}{\varepsilon_u^{\text{th}}}$ (or $\frac{1}{\varepsilon_k^{\text{th}}}$) to explicitly reflect the impact of resource optimization on DEP. Additionally, as BS-HAP-UAV channel attenuation is quite severe, the allocated BS transmit power will be very high to satisfy stringent URLLC requirements. As a result, the BS transmit power will dominate the total BS and UAV transmit power. Nevertheless, this case must be avoided as the UAV is strictly energy-constrained and the UAV transmit power must be carefully controlled. To achieve this aim, we normalized the BS and UAV transmit power by their maximum transmit power, respectively.

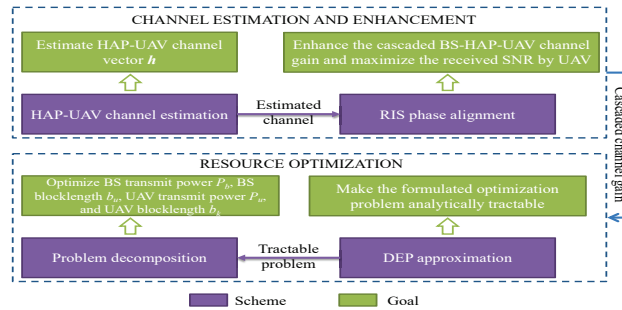


Fig. 2. The flowchat of solving the optimization problem (20).

As different robots may experience diverse channel qualities, we aim at maximizing the minimum system energy efficiency when guaranteeing the stringent URLLC requirements of all robots. We propose to jointly optimize UAV and BS transmit power, blocklength, and RIS phase shift to achieve the goal, under the constraints on DEPs, blocklengths, and UAV and BS transmit power. Combined with the above analysis, the joint resource optimization problem can be formulated as

$$\max_{P_u, P_b, b_u, \{b_k\}, \{\phi_n\}} \min_{k \in \mathcal{K}} \frac{R_u(1 - \epsilon_u) + R_k(1 - \epsilon_k)}{\bar{p}_b + \bar{p}_u} \quad (20a)$$

$$\text{s.t.} : Q(f(b_u, SNR_u)) \leq \varepsilon_u^{\text{th}} \quad (20b)$$

$$\mathbb{E}[Q(f(b_k, SNR_k))] \leq \varepsilon_k^{\text{th}}, \forall k \in \mathcal{K} \quad (20c)$$

$$\phi_n \in [0, 2\pi), \forall n \in \mathbb{N} \quad (20d)$$

$$\text{Constraints (15) -- (18)} \quad (20e)$$

where $\bar{p}_b = P_b/P_B$, $\bar{p}_u = P_u/P_U$, $\epsilon_u = \varepsilon_u/\varepsilon_u^{\text{th}}$, and $\epsilon_k = \varepsilon_k/\varepsilon_k^{\text{th}}$. The solution of (20) is highly challenging for the following reasons: 1) The HAP-UAV channel gain is unknown and needs to be accurately estimated. However, there is a lack of studies on sparse HAP-UAV channel modeling and corresponding accurate channel estimation methods in the literature. 2) There are multiple EM propagation paths in the HAP-UAV channel, and thus, it's difficult to obtain the optimal RIS phase shift such that the received signal strength of the UAV can be maximized. 3) The expression of DEP is highly complex, which makes the problem intractable and greatly hinders the theoretical analysis of the problem. 4) Given the estimated HAP-UAV channel gain, (22) is still difficult to be solved. This is because it contains integer and continuous variables and the decision variables-related to HAP and UAV are intricately coupled, which indicates that the problem is a mixed integer non-convex programming (MINCP) problem.

In this paper, we develop a joint channel estimation, enhancement, and resource optimization framework to solve the above challenging problem, the flowchat of which is shown in Fig. 2. In particular, we first develop a probabilistic channel model to capture the sparsity of the HAP-UAV channel and design a novel channel estimation approach to estimate the HAP-UAV channel with high precision. Second, we design a RIS phase shift optimization strategy that results in a suboptimal HAP-UAV channel gain. Third, we derive the approximate expressions of DEPs to make the problem analytically tractable. Fourth, we analyze the monotonicity of the objective function of the problem. Based on the analysis results, we decompose the problem into two-layered optimization problems, which reduces the difficulty of the theoretical analysis of the problem.

III. HAP-UAV CHANNEL ESTIMATION AND ENHANCEMENT

In this section, we will introduce a message passing-based estimation approach of the HAP-UAV channel¹. The RIS-user channel estimation is a hot and under-studied topic. Recent works in [37]–[39] proposed to use compressed sensing (CS) methods to estimate the RIS-user multi-path channel. However, the authors in [37]–[39] did not discuss

¹The channel estimation mentioned in the paper refers to the small-scale channel estimation without specification. As for large-scale fading, it is usually computed by some deterministic models in multipath channel estimation problems in the research community [37]–[39].

the crucial issue of angle estimation or off-grid angle estimation. As a result, the accuracy of the channel estimation needs to be improved. Here, the HAP-UAV multi-path channel with the off-grid angle consideration will be studied.

For multi-antenna communication systems, with an increasing number of antennas, the spatial resolution in the angular domain will be extended accordingly. As the HAP-UAV channel contains a finite number of propagation paths, the channel will be very sparse in the angular domain. To utilize this sparsity property, we can transform the original channel model into an angular domain representation. In this way, the channel estimation problem is transformed into a sparse signal recovery problem. Generally, we adopt a uniform sampling grid $\hat{\omega} = \{\hat{\omega}_1, \dots, \hat{\omega}_N\}$, which is obtained by discretizing the angular domain $[-\frac{\pi}{2}, \frac{\pi}{2}]$, to match the true AoDs denoted as $\omega = \{\omega_1, \dots, \omega_L\}$ ($L \ll N$). Under the ideal conditions, all of the true AoDs can accurately match grid points. However, the continuous distribution characteristic of the true angle indicates that the grid points cannot effectively capture the true AoDs in practice. Thus, the AoD estimation via an on-grid model usually leads to non-negligible errors. To achieve high-precision estimation results, we introduce off-grid offsets into the on-grid model, which is also called an off-grid model. Specifically, given $\omega_l \notin \{\hat{\omega}_1, \dots, \hat{\omega}_N\}$ and its nearest sampling grid point $\hat{\omega}_{nl} = \min_{n_l \in \{1, \dots, N\}} \{|\omega_l - \hat{\omega}_{n_l}|\}$, we can define the off-grid offset $\Delta\phi_{nl}$ as

$$\Delta\phi_{nl} = \begin{cases} \omega_l - \hat{\omega}_{nl}, & l \in \mathcal{L} = \{1, 2, \dots, L\} \\ 0, & \text{otherwise} \end{cases} \quad (21)$$

The case of $\Delta\phi_{nl} = 0$ indicates that only active paths will be assigned with a non-zero offset (If we don't know the number of true paths in advance, we can set a threshold of path strength to filter non-active paths). Then the corresponding off-grid steering matrix is $\mathbf{A}(\hat{\omega} + \Delta\phi) = [\mathbf{a}(\hat{\omega}_1 + \Delta\phi_1), \dots, \mathbf{a}(\hat{\omega}_N + \Delta\phi_N)]$, and the sparse angular domain channel vector in the complex angular domain is $\mathbf{x} \in \mathbb{C}^N$ with L non-zero elements. Finally, the off-grid sparse angular domain representation of the normalized downlink channel $\bar{\mathbf{h}} \in \mathbb{C}^N$ can be expressed as

$$\bar{\mathbf{h}} = \mathbf{A}(\hat{\omega} + \Delta\phi)\mathbf{x} \triangleq \mathbf{A}(\Delta\phi)\mathbf{x} \quad (22)$$

It's noteworthy that there must be some off-grid offsets making (22) hold. Though it's quite challenging to find the optimal off-grid offsets, the gap between the sampling grid points and the true AoDs will be significantly reduced by iteratively adjusting the off-grid offsets. Therefore, the off-grid model always outweighs the on-grid model.

A. Probability Model of Channel Vector

Recall that the HAP-UAV channel has limited paths in the angular domain. To fully exploit this observation, the probabilistic model of $\mathbf{x} = [x_1, \dots, x_N]^T$ can be modeled by two independent random hidden vectors, i.e., *hidden channel support vector* and *hidden channel value vector*. The *hidden channel support vector* $\mathbf{d} = [d_1, \dots, d_M]^T \in \{0, 1\}^N$ represents the activeness of the paths. Specifically, if $d_n = 1$, then there is an active path around the n -th AoD direction $\hat{\omega}_N + \Delta\phi_N$. We define $p(d_n = 1) = \lambda$, indicating the channel sparsity. The complex-valued *hidden channel value vector* $\mathbf{q} = [q_1, \dots, q_N]^T$ represents the complex gains of paths. $q_n \sim \mathcal{CN}(\zeta, \rho)$ follows an independent and identically distributed (i.i.d.) complex white Gaussian distribution with a mean ζ and variance ρ .

Note that q_n does not determine whether the n -th path from the corresponding AoD direction is active or not. The channel vector can then be expressed as

$$\mathbf{x} = [d_1 q_1, \dots, d_N q_N]^T \quad (23)$$

Accordingly, the joint probabilistic HAP-UAV channel model with a prior distribution can be formulated as

$$p(\mathbf{x}) = p(\mathbf{x}, \mathbf{d}, \mathbf{q}) = p(\mathbf{x}|\mathbf{d}, \mathbf{q})p(\mathbf{d})p(\mathbf{q}) \quad (24)$$

where $p(\mathbf{x}|\mathbf{d}, \mathbf{q})$ is the joint conditional prior. From (24), we know that $p(x_n|d_n, q_n) = 1$ conditioned on $x_n = d_n q_n$; otherwise, $p(x_n|d_n, q_n) = 0$. Thus, $p(\mathbf{x}|\mathbf{d}, \mathbf{q})$ can be expressed as

$$p(\mathbf{x}|\mathbf{d}, \mathbf{q}) = \prod_{n=1}^N p(x_n|d_n, q_n) = \prod_{n=1}^N \delta(x_n - d_n q_n) \quad (25)$$

where $\delta(\cdot)$ is the Dirac delta function.

B. Problem Formulation of Off-Grid Sparse Channel Estimation

Using the angular domain channel representation, we can rewrite (2) as a standard CS model

$$\mathbf{y} = \mathbf{F}(\Delta\phi)\mathbf{x} + \mathbf{n}_e \quad (26)$$

where $\mathbf{F}(\Delta\phi) = \mathbf{U}_0^H \bar{\mathbf{H}}^H \Theta^H \mathbf{A}(\Delta\phi) \in \mathbb{C}^{P \times N}$ is the measurement matrix, $\bar{\mathbf{H}}$ is the normalized BS-HAP channel matrix, $\mathbf{U}_0 \in \mathbb{C}^{M \times P}$ is a training pilot matrix from the BS, $\mathbf{n}_e \sim \mathcal{CN}(0, \sigma_e^2 \mathbf{I})$ is the complex AWGN. In terms of a CS problem, the choice of measurement matrix has a direct influence on the desired performance of the recovery approach. In the proposed model, we design pilot \mathbf{U}_0 based on the partial discrete Fourier transform (DFT) random permutation (pDFT-RP) measurement matrix. The following Lemma presents how to generate the pilot matrix \mathbf{U}_0 .

Lemma 1. For any off-grid offset $\Delta\phi$, the pilot matrix to be transmitted by the BS can be expressed as

$$\mathbf{U}_0^H = \mathbf{S} \mathbf{D} \mathbf{R} (\bar{\mathbf{H}}^H \Theta^H \mathbf{A}(\mathbf{0}))^{-1} \quad (27)$$

Proof. Please refer to Appendix A. □

We can then estimate the off-grid sparse channel with (26). Besides, we leverage the minimum mean square error (MMSE) criterion to evaluate the estimation performance. The estimated complex gain is $\hat{x}_n = E(x_n|\mathbf{y}, \Delta\phi)$, which will result in the MMSE. The expectation is taken over the marginal posterior $p(x_n|\mathbf{y}, \Delta\phi)$ given measurements \mathbf{y} and off-grid offsets $\Delta\phi$. To exploit the inherent statistical structure of the HAP-UAV channel in terms of channel support and value vectors, the marginal posterior distribution can be expressed by Bayes' rule as

$$p(x_n|\mathbf{y}, \Delta\phi) \propto \sum_{\mathbf{d}} \int_{\mathbf{x}_{-n}, \mathbf{q}} p(\mathbf{x}, \mathbf{d}, \mathbf{q}|\mathbf{y}, \Delta\phi) = \sum_{\mathbf{d}} \int_{\mathbf{x}_{-n}, \mathbf{q}} p(\mathbf{d})p(\mathbf{q}) \prod_{n=1}^N p(x_n|d_n, q_n) \prod_{p=1}^P p(y_p|\mathbf{x}, \Delta\phi) \quad (28)$$

where \propto indicates proportionality up to a constant scale factor, \mathbf{x}_{-n} means a vector \mathbf{x} excluding the element x_n . According to (26), the likelihood function $p(y_p|\mathbf{x}, \Delta\phi) = \mathcal{CN}(y_p; \mathbf{f}_p \mathbf{x}, \sigma_e^2)$, where \mathbf{f}_p is the p -th row of measurement matrix \mathbf{F} . The optimal off-grid offsets $\Delta\phi$ can be obtained by a maximum likelihood (ML) approach

$$\Delta\phi^* = \arg \max_{\Delta\phi} \ln p(\mathbf{y}, \Delta\phi) = \arg \max_{\Delta\phi} \ln \int_{\mathbf{x}} p(\mathbf{x}, \mathbf{y}, \Delta\phi) d\mathbf{x} \quad (29)$$

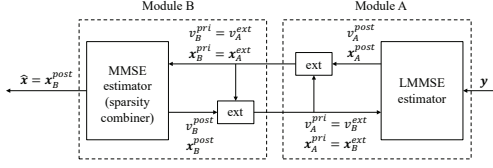


Fig. 3. Two recurrent modules of the R-OAMP approach.

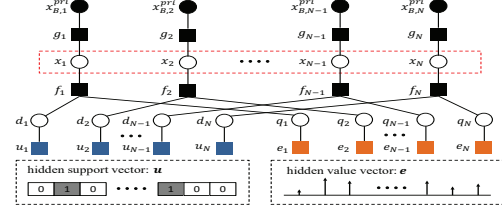


Fig. 4. A factor graph of hidden channel support and value vectors.

After obtaining the estimated offsets $\Delta\phi^*$, we can then calculate the corresponding marginal posterior distribution (28). It's the production of many distribution functions, each of which is determined by only a subset of variables. Such decomposition structures can be calculated by a graphical model, i.e., a factor graph, which can be an undirected bipartite graph used to represent the connection between random variables (called variable nodes) and related probability density functions (pdfs) (called factor nodes). Unfortunately, in (28), the generated factor graph contains a densely connected structure due to the measurement matrix, which underestimates the exact calculation of the posterior distribution using the factor graph. To handle this challenge, we propose a Recurrent-OAMP approach that can decouple the linear and nonlinear observations in the following subsection.

C. Recurrent-OAMP Approach

The Recurrent-OAMP approach contains two iteratively working modules, as shown in Fig. 3: Module A is a linear MMSE (LMMSE) estimator, inputting observations and messages from Module B; Module B is an MMSE estimator, inputting the inherent sparse prior and messages from Module A. Both modules will work iteratively until convergence.

1) *Module A: LMMSE Estimator:* In Module A, since only linear observations are considered, we can consider that \mathbf{x} has a Gaussian distribution with mean \mathbf{x}_A^{pri} and variance v_A^{pri} passed from module B without a sparse prior. Given received signals \mathbf{y} and the prior distribution $\mathcal{CN}(\mathbf{x}; \mathbf{x}_A^{pri}, v_A^{pri} \mathbf{I})$, the LMMSE estimation \mathbf{x}_A^{post} and its mean squared error (MSE) v_A^{post} are respectively given by [40]

$$\mathbf{x}_A^{post} = \mathbf{x}_A^{pri} + \frac{v_A^{pri}}{v_A^{pri} + \sigma_e^2} \mathbf{F}(\Delta\phi)^H (\mathbf{y} - \mathbf{F}(\Delta\phi) \mathbf{x}_A^{pri}) \quad (30)$$

$$v_A^{post} = v_A^{pri} - \frac{P}{N} \cdot \frac{(v_A^{pri})^2}{v_A^{pri} + \sigma_e^2} \quad (31)$$

As $\mathcal{CN}(\mathbf{x}; \mathbf{x}_A^{post}, v_A^{post} \mathbf{I})$ and $\mathcal{CN}(\mathbf{x}; \mathbf{x}_A^{pri}, v_A^{pri} \mathbf{I})$ are independent of each other, the extrinsic message is also subject of a Gaussian distribution and given by

$$\mathcal{CN}(\mathbf{x}; \mathbf{x}_A^{post}, v_A^{post} \mathbf{I}) \propto \mathcal{CN}(\mathbf{x}; \mathbf{x}_A^{pri}, v_A^{pri} \mathbf{I}) \mathcal{CN}(\mathbf{x}; \mathbf{x}_A^{ext}, v_A^{ext} \mathbf{I}) \quad (32)$$

Hence, the extrinsic mean and variance can be computed by [40]

$$\mathbf{x}_B^{pri} = \mathbf{x}_A^{ext} = v_A^{ext} \left(\frac{\mathbf{x}_A^{post}}{v_A^{post}} - \frac{\mathbf{x}_A^{pri}}{v_A^{pri}} \right) \quad (33)$$

$$v_B^{pri} = v_A^{ext} = \left(\frac{1}{v_A^{post}} - \frac{1}{v_A^{pri}} \right)^{-1} \quad (34)$$

where \mathbf{x}_B^{pri} and v_B^{pri} are the input mean and variance of Module B, which are equal to \mathbf{x}_A^{ext} and v_A^{ext} , respectively.

2) *Module B: MMSE Estimator:* In Module B, the MMSE estimator is designed with proposed sparsity channel priors. However, an MMSE estimator in the OAMP approach performs estimation based on i.i.d. priors, which thus cannot be directly applied. Therefore, we need to re-design the MMSE estimator by fully exploiting the sparsity structure in the HAP-UAV channel. For the investigated sparse signal recovery approach, a basic assumption is that the extrinsic message \mathbf{x}_B^{pri} is achieved by an approximated additive white Gaussian noise (AWGN) observation of \mathbf{x} , mathematically,

$$\mathbf{x}_B^{pri} = \mathbf{x} + \mathbf{z} \quad (35)$$

where $\mathbf{z} \sim \mathcal{CN}(0, v_B^{pri} \mathbf{I})$ is independent of \mathbf{x} . Extensive experiments have proved that the AWGN observation assumption is valid for OAMP [41]. Additionally, if constructing a factor graph with (35) rather than the joint distribution $p(\mathbf{x}, \mathbf{d}, \mathbf{q}, \mathbf{y})$, the computational complexity of each iteration of a message passing approach running on the factor graph decreases dramatically to $O(N)$. Therefore, based on (35), the factor graph of the joint distribution $p(\mathbf{x}, \mathbf{d}, \mathbf{q}, \mathbf{x}_B^{pri})$ denoted by \mathcal{J} can be shown in Fig. 4, where the functional form of each factor node is listed as below: $g_n(x_n, x_{B,n}^{pri}) \sim p(x_{B,n}^{pri} | x_n) = \mathcal{CN}(x_n; x_{B,n}^{pri}, v_B^{pri})$, $f_n(x_n, d_n, q_n) \sim p(x_n | d_n, q_n) = \delta(x_n - d_n q_n)$, $u_n(d_n) \sim p(d_n) = (1 - \lambda)^{1-d_n} \lambda^{d_n}$, $e_n(q_n) \sim p(q_n) = \mathcal{CN}(q_n; \zeta, \rho)$. Our goal is to calculate the marginal posterior distribution $\left\{ p(x_n | \mathbf{x}_B^{pri}) \right\}_{n=1}^N$ by message passing on the graph \mathcal{J} . As the graph \mathcal{J} does not contain loops, we can directly explore sum-product message passing rules without additional approximation. The details of the message scheduling are as below.

Step 1: According to the sum-product algorithm, the message from factor node g_n to variable node x_n is

$$\eta_{g_n \rightarrow x_n}(x_n) = p(x_{B,n}^{pri} | x_n) = \mathcal{CN}(x_n; x_{B,n}^{pri}, v_B^{pri}) \quad (36)$$

Step 2: Given prior information, compute the message from variable node q_n to factor node f_n , i.e.,

$$\eta_{q_n \rightarrow f_n}(q_n) = \mathcal{CN}(q_n; \zeta, \rho) \quad (37)$$

Step 3: According to sum-product rules, the message from factor node f_n to variable node x_n is

$$\eta_{f_n \rightarrow x_n}(x_n) = \frac{\sum_{d_n} \int_{q_n} \eta_{q_n \rightarrow f_n}(q_n) \eta_{d_n \rightarrow f_n}(d_n) \delta(x_n - d_n q_n) dq_n}{\sum_{d_n} \int_{q_n} \eta_{q_n \rightarrow f_n}(q_n) \eta_{d_n \rightarrow f_n}(d_n) \delta(x_n - d_n q_n) dq_n dx_n} = (1 - \lambda) \delta(x_n) + \lambda \mathcal{CN}(\delta(x_n); \zeta, \rho) \quad (38)$$

It should be noted that (38) is a Bernoulli-Gaussian distribution. With just three parameters $\{\lambda, \zeta, \rho\}$, we can control the distribution of x_n . In practice, even though we can't predict these parameters, we can estimate their values by some methods (e.g., expectation-maximization).

Step 4: Then, the posterior distribution can be given by

$$p(x_n | \mathbf{x}_B^{pri}) \propto \eta_{f_n \rightarrow x_n}(x_n) \eta_{g_n \rightarrow x_n}(x_n) \quad (39)$$

According to the principle of MMSE, the posterior mean and variance can be respectively computed by

$$x_{B,n}^{post} = E(x_n | \mathbf{x}_B^{pri}) = \int_{x_n} x_n p(x_n | \mathbf{x}_B^{pri}) \quad (40)$$

$$v_B^{post} = \frac{1}{N} \sum_{n=1}^N \text{Var}(x_n | \mathbf{x}_B^{pri}) = \frac{1}{N} \sum_{n=1}^N \int_{x_n} |x_n - \mathbb{E}(x_n | \mathbf{x}_B^{pri})|^2 p(x_n | \mathbf{x}_B^{pri}) \quad (41)$$

After updating the posterior distribution of \mathbf{x} , the extrinsic update mean and covariance passed to Module A can be expressed as

$$\mathbf{x}_A^{pri} = \mathbf{x}_B^{ext} = v_B^{ext} \left(\frac{\mathbf{x}_B^{post}}{v_B^{post}} - \frac{\mathbf{x}_B^{pri}}{v_B^{pri}} \right) \quad (42)$$

$$v_A^{pri} = v_B^{ext} = \left(\frac{1}{v_B^{post}} - \frac{1}{v_B^{pri}} \right)^{-1} \quad (43)$$

When the posterior distribution is obtained by message passing in Module B, the extrinsic message will be sent back to module A. This message-passing pattern is similar to how a recurrent network works, so the recurrent-OAMP (R-OAMP) approach is named. R-OAMP executes message passing between Module A and Module B until convergence.

Once the estimated posterior distribution $\hat{p}(\mathbf{x} | \mathbf{y}, \Delta\phi) = \prod_{n=1}^N p(x_n | \mathbf{y}, \Delta\phi)$ is obtained, we can update the off-grid offsets $\Delta\phi$ using ML. Unfortunately, we can't obtain the closed-form expression of the log-likelihood function $\ln p(\mathbf{y}, \Delta\phi)$. As a result, the gradient descent method can't be directly utilized to derive the optimal solution $\Delta\phi^*$. To address this challenging issue, we utilize the in-exact majorization-minimization (MM) algorithm in [42] to approximate the optimal solution, which guarantees to converge to a stationary point [43]. Specifically, let the surrogate function of $\ln p(\mathbf{y}, \Delta\phi)$ be $r(\Delta\phi; \Delta\dot{\phi})$, which indicates that this progressively refined function is constructed at a given point $\Delta\dot{\phi}$. As the lower bound, $r(\Delta\phi; \Delta\dot{\phi})$ should satisfy the following three conditions:

$$r(\Delta\phi; \Delta\dot{\phi}) \leq \ln p(\mathbf{y}, \Delta\phi), \forall \Delta\phi \quad (44)$$

$$r(\Delta\dot{\phi}; \Delta\dot{\phi}) = \ln p(\mathbf{y}, \Delta\dot{\phi}) \quad (45)$$

$$\left. \frac{\partial r(\Delta\phi; \Delta\dot{\phi})}{\partial \Delta\phi} \right|_{\Delta\phi=\Delta\dot{\phi}} = \left. \frac{\partial \ln p(\mathbf{y}, \Delta\phi)}{\partial \Delta\phi} \right|_{\Delta\phi=\Delta\dot{\phi}} \quad (46)$$

It's not hard to verify that the following constructed progressively refined function satisfies all the above conditions

$$r(\Delta\phi; \Delta\dot{\phi}) = \int p(\mathbf{x} | \mathbf{y}, \Delta\dot{\phi}) \ln \frac{p(\mathbf{x}, \mathbf{y}, \Delta\phi)}{p(\mathbf{x} | \mathbf{y}, \Delta\dot{\phi})} d\mathbf{x} \quad (47)$$

With the constructed function, we can iteratively update $\Delta\phi$ by

$$\Delta\phi^{i+1} = \arg \max_{\Delta\phi} r(\Delta\phi; \Delta\phi^i) \quad (48)$$

where i represents the i -th iteration and $\Delta\phi^i$ stands for the corresponding value of $\Delta\phi$.

Nevertheless, it's quite difficult to obtain the optimal $\Delta\phi^{i+1}$ as (48) is non-convex. To solve this problem effectively, we explore a gradient ascend method, and $\Delta\phi^{i+1}$ can be updated by

$$\Delta\phi^{i+1} = \Delta\phi^i + \alpha_i \left. \frac{\partial r(\Delta\phi; \Delta\phi^i)}{\partial \Delta\phi} \right|_{\Delta\phi=\Delta\phi^i} \quad (49)$$

where α_i is the update stepsize. Besides, to obtain high-precision estimation results, we utilize the backtracking linear search method, which can avoid oscillating results or slow convergence by adaptively adjusting the stepsize.

Please refer to Appendix B. for the detailed update expression of off-grid offsets $\Delta\phi^{i+1}$.

Algorithm 1 Recurrent-OAMP

- 1: **Input:** Received signal (or observations) \mathbf{y} , measurement matrix $\mathbf{F}(0)$, noise variance σ_e^2 , $I_c^{\max} = 50$.
 - 2: **Initialize:** $\mathbf{x}_A^{pri} = \mathbf{0}$, $v_A^{pri} = \lambda\rho$, $\Delta\phi = \mathbf{0}$
 - 3: **while** not converge **do**
 - 4: **Module A (given $\Delta\phi = \Delta\phi^i$):**
 - 5: Update \mathbf{x}_A^{post} and v_A^{post} using (30) and (31).
 - 6: Update $\mathbf{x}_B^{pri} = \mathbf{x}_A^{ext}$ and $v_B^{pri} = v_A^{ext}$ using (33) and (34).
 - 7: **Module B:**
 - 8: Message passing over the path $g_n \rightarrow x_n$ using (36) with outputs of Module A.
 - 9: Message passing over the path $q_n \rightarrow f_n$ using (37).
 - 10: Message passing over the path $f_n \rightarrow x_n$ using (38).
 - 11: Calculate the posterior distribution $f_n \rightarrow x_n$ using (39), and update \mathbf{x}_B^{post} and v_B^{post} using (40) and (41).
 - 12: Update $\mathbf{x}_A^{pri} = \mathbf{x}_B^{ext}$ and $v_A^{pri} = v_B^{ext}$ using (42) and (43).
 - 13: Repeat Module A and Module B until convergence.
 - 14: Output $\hat{p}(x|\mathbf{y}, \Delta\phi^i) = \mathcal{CN}(x_n; \mathbf{x}_B^{post}, v_B^{post} \mathbf{I})$
 - 15: **Off-grid Estimation:**
 - 16: Update off-grid offsets $\Delta\phi^{i+1}$ using (83).
 - 17: Update $i = i + 1$.
 - 18: **end while**
 - 19: **Output:** $\hat{\mathbf{x}} = \mathbf{x}_B^{post}$ and $\hat{\mathbf{h}} = \mathbf{A}(\Delta\phi^{i+1})\hat{\mathbf{x}}$.
-

D. Channel Enhancement via RIS Phase Alignment

In this subsection, we discuss how to enhance the HAP-UAV channel by aligning RIS phases. The optimization of RIS phase shift is crucial for the performance improvement of RIS-integrated communication systems. By aligning the phase shift Θ , signals sent by the BS and then reflected by the RIS can be coherently added to the UAV, which thus significantly increase the HAP-UAV channel gain and maximize the received SNR by the UAV SNR_u .

Given the estimated HAP-UAV channel vector \mathbf{h} , we can then formulate the RIS phase shift optimization problem as $\Theta^* = \arg \max_{\Theta} \frac{P_b G}{\sigma_0^2} |\mathbf{h}^H \Theta \mathbf{H} \mathbf{v}|^2$, where σ_0^2 is the noise power. To achieve the optimal Θ , we first need to determine the precoding vector \mathbf{v} . The following Lemma presents a strategy for designing the precoding vector.

Lemma 2. For any given BS-HAP-UAV propagation channel and RIS phase shift, the BS needs to adopt a maximum ratio transmission (MRT) strategy to maximize SNR_u , that is, we have

$$\mathbf{v} = \frac{\mathbf{a}_{BS}(v_{AoD})}{\|\mathbf{a}_{BS}(v_{AoD})\|_2} \quad (50)$$

Proof. Please refer to Appendix C. □

Using (50), SNR_u can be rewritten as

$$SNR_u = \frac{P_b G}{\sigma_0^2} \left| \mathbf{h}^H \mathbf{\Theta} \mathbf{H} \frac{\mathbf{a}_{BS}(v_{AoD})}{\|\mathbf{a}_{BS}(v_{AoD})\|_2} \right| = \frac{\alpha P_b G}{\sigma_0^2} \left| \sum_{n=1}^N \sum_{l=1}^L \beta_l e^{j(\theta_n + 2\pi(n-1)\bar{d}_{RIS}(\sin(\omega_l) - \sin(v_{AoA}))} \right|^2 \quad (51)$$

where β_l is the product of the l -th non-zero element of the estimated small-scale channel fading $\hat{\mathbf{x}}$ and the large-scale channel fading of the HAP-UAV channel.

From (51), we can find that SNR_u is independent of AoD v_{AoD} . However, as there are multiple reflected/scattered paths in the HAP-UAV EM propagation environment, it's difficult to optimize θ_n ($\forall n$) that can maximize the received signal power of the UAV. Hence, we attempt to obtain the suboptimal θ_n ($\forall n$). To this end, we rearrange (51) as

$$SNR_u = \frac{\alpha P_b G}{\sigma_0^2} \left| \sum_{l=1}^L \beta_l r_l \right|^2 \quad (52)$$

where $r_l \triangleq \left| \sum_{n=1}^N e^{j(\theta_n + 2\pi(n-1)\bar{d}_{RIS}(\sin(\omega_l) - \sin(v_{AoA}))} \right|^2$.

Therefore, maximizing (52) is equivalent to maximizing $\{r_l\}_{l \in \mathcal{L}}$. Denote l_0 as the phase alignment path of RIS and $\psi_n^*(l_0)$ the corresponding phase shift. Then, we can coherently reflect signals via path l_0 by setting

$$\psi_n^*(l_0) = \theta - 2\pi(n-1)\bar{d}_{RIS}(\sin(\omega_{l_0}) - \sin(v_{AoA})) \quad (53)$$

where $\theta \in [0, 2\pi)$ is an arbitrary phase shift. By enforcing

$$\theta_n = \psi_n^*(l_0) \quad (54)$$

and performing specific mathematical transformations, we can then rewrite r_l as

$$r_l = g(\Delta\psi_l(l_0)) \triangleq \left| \frac{\sin(\pi N \bar{d}_{RIS} \Delta\psi_l(l_0))}{\sin(\pi \bar{d}_{RIS} \Delta\psi_l(l_0))} \right|^2 \quad (55)$$

where $\Delta\psi_l(l_0) = \sin(\omega_l) - \sin(\omega_{l_0})$. To maximize (55), we need to minimize $|\Delta\psi_l(l_0)|$. Considering the low-latency requirement of URLLC services, we perform the first-order Taylor expansion on $|\Delta\psi_l(l_0)|$ to realize the rapid configuration of RIS phase shift, i.e.,

$$|\Delta\psi_l(l_0)| \approx |\cos(\omega_l)| |\omega_l - \omega_{l_0}| \quad (56)$$

As a result, we can reformulate the RIS Phase shift optimization problem as

$$\min_{\omega_{l_0}, \zeta_l} \sum_{l=1}^L |\beta_l \cos(\omega_l)| \zeta_l \quad (57a)$$

$$\text{s.t.} : \omega_{l_0} - \zeta_l \leq \omega_l, \forall l \in \mathcal{L} \quad (57b)$$

$$\omega_l \leq \omega_{l_0} + \zeta_l, \forall l \in \mathcal{L} \quad (57c)$$

(57) is a linear programming problem and can then be efficiently solved by optimization tools such as MOSEK.

IV. RESOURCE OPTIMIZATION AND ALGORITHM DESIGN

We next discuss how to solve the original optimization problem with the cascaded BS-HAP-UAV channel gain. As mentioned above, the complicated DEP expression greatly hinders the theoretical analysis of the optimization problem. Therefore, we first attempt to approximate the DEP.

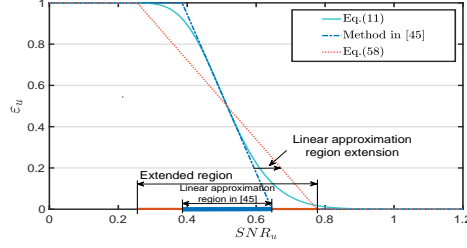


Fig. 5. The function ε_u in comparison with its two types of approximations.

A. DEP Approximation

To obtain an analysis-friendly expression of DEP ε_u , we improve the linear approximation method in [44]. The key idea of this method is to conduct the first-order Taylor series expansion at the point $SNR_u = \gamma_u$ to achieve an asymptotical expression. Different from the approximation in [44], we extend the linear approximation region and propose to allocate redundant resources to achieve a lower DEP, as shown in Fig. 5. Specifically, we approximate ε_u as

$$\varepsilon_u \approx \Omega(SNR_u) = \begin{cases} 1, & SNR_u \leq SNR_{low} \\ 0, & SNR_u \geq SNR_{up} \\ \frac{1}{2} - \frac{1}{2\chi_u}(SNR_u - \gamma_u), & \text{otherwise} \end{cases} \quad (58)$$

where $\gamma_u = 2^{R_u} - 1$, $SNR_{low} = \gamma_u - \frac{1}{\chi_u}$, $SNR_{up} = \gamma_u + \frac{1}{\chi_u}$, and $\chi_u = \sqrt{\frac{b_u}{2\pi}}(2^{2R_u} - 1)^{-1/2}$. Similarly, $\Omega(SNR_k)$ represents the Taylor series expansion based approximation of $Q(f(b_k, SNR_k))$.

Recall that the UtG channel is a random channel. However, the UtG channel fading should be regarded as a constant during a transmission interval. Thus, we need to analyze the expected DEP, denoted by $\bar{\varepsilon}_k$, experienced by any robot k , which can be calculated by

$$\bar{\varepsilon}_k = \mathbb{E}[Q(f(b_k, SNR_k))] \approx \int_0^\infty \Omega(SNR_k) f_{SNR_k}(x) dx = \chi_k \int_{\gamma_k - \frac{1}{\chi_k}}^{\gamma_k + \frac{1}{\chi_k}} F_{SNR_k}(x) dx \quad (59)$$

where $f_{SNR_k}(x)$ and $F_{SNR_k}(x)$ are the pdf and the cdf of SNR_k , respectively.

As the Rayleigh small-scale fading is considered, SNR_k follows an exponential distribution. Thus, $F_{SNR_k}(x)$ can be computed by [45]

$$F_{SNR_k}(x) = \begin{cases} 1 - e^{-\frac{x}{\overline{SNR_k}}}, & x > 0 \\ 0, & x \leq 0 \end{cases} \quad (60)$$

where $\overline{SNR_k} = P_u |g_k^L|^2 / \sigma_k^2$ is the average value of SNR_k .

By substituting (60) into (59), for any robot $k \in \mathcal{K}$, we can calculate its expected DEP by

$$\bar{\varepsilon}_k \approx \chi_k \int_{\gamma_k - \frac{1}{\chi_k}}^{\gamma_k + \frac{1}{\chi_k}} (1 - e^{-x/\overline{SNR_k}}) dx \stackrel{(a)}{\approx} \frac{2\gamma_k}{\overline{SNR_k}} \quad (61)$$

where (a) follows from the approximation $1 - e^{-x/\overline{SNR_k}} \approx \frac{x}{\overline{SNR_k}}$ under an assumption of high SNR [45]. This assumption is reasonable for URLLC applications because robots need to achieve high SNR such that the stringent QoS requirements can be satisfied.

B. Original Problem Decomposition

After obtaining the estimated HAP-UAV channel gain, the aligned RIS phase, and the approximated DEPs, the original problem (20) becomes analytically tractable. Nevertheless, we observe that there are integer and continuous variables in (20) and the decision variables are complexly coupled. (20) can be confirmed to be a MINCP problem, which is challenging. Generally, resorting to an iterative optimization scheme is a feasible way of solving this challenging problem. Yet, the developed algorithm would contain multiple nested loops if we directly adopt the iterative optimization scheme, which increases the computational complexity of the algorithm.

Fortunately, given a BS blocklength b , we observe that the optimal P_b does not vary with the UAV transmit power P_u . This is because there is a narrow feasible region $\hat{\mathcal{D}}_p \subseteq \mathcal{D}_p = \{P_b \mid Q(f(b_u, SNR_u)) \leq \varepsilon_u^{\text{th}}, 0 < P_b \leq P_B\}$, in which $\Omega(SNR_u)$ strictly monotonically decreases with P_b . Given the blocklength b , the objective function (20a) then reduces to a monotonically increasing function over P_b in the specific feasible region $\hat{\mathcal{D}}_p$.

Therefore, we can apply horizontal decomposition to (20) that creates a problem of two-layered structure. The 1st layer is *BS-Layer Optimization*, and the 2nd layer is *UAV-Layer Optimization*. More importantly, we need not to conduct iterative optimization between these two layers.

1) *BS-Layer Optimization*: Given any decision variables-related to the UAV-Layer Optimization, we can formulate the BS-Layer Optimization problem as

$$\max_{P_b} \min_{k \in \mathcal{K}} \frac{R_u(1 - \epsilon_u) + R_k(1 - \epsilon_k)}{\bar{p}_b + \bar{p}_u} \quad (62a)$$

$$\text{s.t.} : \Omega(SNR_u) \leq \varepsilon_u^{\text{th}} \quad (62b)$$

$$\text{Constraints (15), (17)} \quad (62c)$$

where $\min\{x_k\}$ denotes the minimum x_k , $\forall k \in \mathcal{K}$.

We observe from the expressions of R_u and $\Omega(SNR_u)$ that the decision variables P_b and b_u in (62) are intricately coupled, which challenges the solution to (62). To tackle this issue, we propose to decompose (62) into two subproblems, named *BS transmit power control* subproblem and *BS blocklength optimization* subproblem.

1-a) BS transmit power control: Given b_u , P_u and $\{b_k\}$, the BS power control subproblem can be reduced to

$$\max_{P_b} \min_{k \in \mathcal{K}} \frac{R_u(1 - \epsilon_u) + R_k(1 - \epsilon_k)}{\bar{p}_b + \bar{p}_u} \text{ s.t. : Constraints (17), (62b)} \quad (63a)$$

Recall that $\Omega(SNR_u)$ is a piecewise function. Thus, we need to discuss the power control subproblem in three different cases closely related to the value of SNR_u . We can directly exclude the case of $SNR_u \leq \gamma_u - \frac{1}{\chi_u}$ as it will result in an unacceptable DEP. Then, we discuss the remaining two cases, respectively.

Case I: ($SNR_u \geq SNR_{\text{up}}$) In this case, we have $\varepsilon_u = 0$, and the BS power control subproblem can be reformulated as

$$\max_{P_b} \min_{k \in \mathcal{K}} \frac{R_u + R_k(1 - \epsilon_k)}{\bar{p}_b + \bar{p}_u} \quad (64a)$$

$$\text{s.t.} : \bar{p}_b \geq SNR_{\text{up}} / (P_B \Delta B) \quad (64b)$$

$$\text{Constraint (17)}. \quad (64c)$$

where $\Delta B = G|\mathbf{h}^H \mathbf{\Theta} \mathbf{H} \mathbf{v}|^2 / \sigma_0^2$. As the numerator of (64a) is not related to \bar{p}_u , the objective function of (64) monotonically decreases with P_b . Thus, given b_k , the optimized BS transmit power (denoted by $P_b(b_k)$) can be computed by

$$P_b(b_u) = \min \{P_B, SNR_{up}/\Delta B\} \quad (65)$$

Case II: ($SNR_{low} < SNR_u < SNR_{up}$) In this case, We can reformulate (63) as

$$\max_{P_b} \min_{k \in \mathcal{K}} \frac{R_u(1 - \epsilon_u) + R_k(1 - \epsilon_k)}{\bar{p}_b + \bar{p}_u} \quad (66a)$$

$$\text{s.t.} : SNR_{low}/(P_B \Delta B) \leq \bar{p}_b \leq SNR_{up}/(P_B \Delta B) \quad (66b)$$

$$\text{Constraint (17)}. \quad (66c)$$

Generally, the monotonicity of (66a) is hard to be determined. Fortunately, we observe that the feasible region \mathcal{P}_b of (66) is rather narrow, in which the numerator of (66a) varies greatly, while the denominator remains almost unchanged. Therefore, the monotonicity of (66a) is dominated by its numerator. The numerator is then a monotonically increasing function in \mathcal{P}_b , and so is (66a). It further indicates that the two discussed cases have the same solution that is given in (65).

1-b) BS blocklength optimization problem: Given $P_b(b_u)$, P_u , and $\{b_k\}$, we can formulate the BS blocklength optimization problem as

$$\max_{b_u} \min_{k \in \mathcal{K}} \frac{R_u(1 - \epsilon_u) + R_k(1 - \epsilon_k)}{P_b(b_u)/P_B + \bar{p}_u} \text{ s.t. : Constraints (15), (62b)}. \quad (67a)$$

Note that the obtained $P_b(b_u)$ is a function of b_u . After substituting $P_b(b_u)$ into (67), we can obtain an objective function regarding variable b_u . However, the obtained objective function is non-concave even given a relaxed variable b_u . Fortunately, considering that the feasible region of (67) is small, it will be a good choice to achieve its optimal solution by exhaustively searching.

Remark 2: Observe that the optimized $P_b(b_u)$ is a function b_u . After obtaining b_u using an exhaustive search method, we can directly obtain the optimized $P_b(b_u)$ by (65). It indicates that we can solve the *BS-Layer Optimization* problem in just two iterations.

2) *UAV-Layer Optimization:* Given any decision variables related to the BS-Layer Optimization, we can formulate the UAV-Layer Optimization problem as

$$\max_{P_u, \{b_k\}} \min_{k \in \mathcal{K}} \frac{R_u(1 - \epsilon_u) + R_k(1 - \epsilon_k)}{\bar{p}_b + \bar{p}_u} \quad (68a)$$

$$\text{s.t.} : 2\gamma_k / \overline{SNR_k} \leq \epsilon_k^{\text{th}}, \forall k \in \mathcal{K} \quad (68b)$$

$$\text{Constraints (16), (18)} \quad (68c)$$

Similarly, as (68) is a mixed-integer optimization problem, we decompose it into two iteratively optimized subproblems, i.e., *UAV transmit power control* subproblem and *UAV blocklength optimization* subproblem, such that (68) can be effectively solved.

2-a) UAV transmit power control: Assuming that the values of the blocklength of b_k , $\forall k$, P_b , and b_u are given, we can then formulate the UAV transmit power control subproblem as

$$\max_{P_u} \eta_{EE} = \min_{k \in \mathcal{K}} \frac{R_u(1 - \epsilon_u) + R_k(1 - \epsilon_k)}{\bar{p}_b + \bar{p}_u} \text{ s.t : Constraints (18), (68b)}. \quad (69a)$$

The objective function of (69) is a complex fraction, which makes it hard to be directly optimized. To address this issue, we define the optimal η_{EE}^* as

$$\eta_{EE}^* = \min_{k \in \mathcal{K}} \frac{R_u(1 - \epsilon_u) + R_k(\bar{p}_u^*)(1 - \epsilon_k(\bar{p}_u^*))}{\bar{p}_b + \bar{p}_u^*} \quad (70)$$

where $\bar{p}_u^* = P_u^*/P_U$ is the optimal solution of (69). The following Lemma presents how to calculate η_{EE}^* .

Lemma 3. η_{EE}^* can be achieved if and only if

$$\begin{aligned} & \max_{P_u} \min_{k \in \mathcal{K}} R_u(1 - \epsilon_u) + R_k(1 - \epsilon_k) - \eta_{EE}^* (\bar{p}_b + \bar{p}_u) \\ &= \min_{k \in \mathcal{K}} R_u(1 - \epsilon_u) + R_k(\bar{p}_u^*)(1 - \epsilon_k(\bar{p}_u^*)) - \eta_{EE}^* (\bar{p}_b + \bar{p}_u^*) \\ &= 0 \end{aligned} \quad (71)$$

Proof. Please refer to Appendix D. □

According to **Lemma 3**, we can transform the expression of the objective function of (69). As a result, (69) can be equivalently transformed into

$$\max_{P_u} \min_{k \in \mathcal{K}} R_u(1 - \epsilon_u) + R_k(1 - \epsilon_k) - \eta_{EE}(\bar{p}_b + \bar{p}_u) \quad (72a)$$

$$\text{s.t : } \bar{p}_u \geq 2\gamma_k \sigma_k^2 / (|g_k^L|^2 \varepsilon_k^{\text{th}} P_U), \forall k \in \mathcal{K} \quad (72b)$$

$$\text{Constraint (18)}. \quad (72c)$$

Note that (72) is a typical max-min optimization problem. Then, we introduce an auxiliary variable y and equivalently transform (72) into

$$\max_{P_u, y} y \quad (73a)$$

$$\text{s.t : } 2\gamma_k \sigma_k^2 / (|g_k^L|^2 \bar{p}_u P_U) \leq 1 + (R_u(1 - \epsilon_u) - y - \eta_{EE}(\bar{p}_b + \bar{p}_u)) / R_k, \forall k \in \mathcal{K} \quad (73b)$$

$$\text{Constraints (18), (72b)}. \quad (73c)$$

It can be confirmed that (73) is a rotated quadratic cone programming problem that can be efficiently optimized by some commercial optimization tools such as MOSEK. Therefore, we can conclude the steps of optimizing (69) in the Algorithm 2.

2-b) UAV blocklength optimization Given the UAV transmit power P_u , we can formulate the UAV blocklength optimization subproblem as

$$\max_{\{b_k\}} \min_{k \in \mathcal{K}} R_k(1 - \epsilon_k) \text{ s.t : Constraints (16), (68b)} \quad (76a)$$

Note that (76) is a non-linear integer programming problem. The computational complexity of solving it using some traditional optimization methods is extremely high. Nevertheless, the feasible region of (76) is small. Then,

Algorithm 2 UAV Transmit Power Control

1: **Initialization:** Initialize $\eta_{\text{EE}}^{(0)}$ and $y^{(0)}$. Let error tolerance parameter $\Delta_r = 1\text{e} - 3$, maximum iterations $r_{\text{max}} = 50$, and $r = 0$. Input $\{b_k\}$ and the optimized b_u and P_b .

2: **repeat**

3: Given $\eta_{\text{EE}}^{(r)}$, solve (73) to obtain the optimized UAV transmit power $P_u^{(r+1)}$ using the MOSEK tool.

4: Given $P_u^{(r+1)}$ and $\eta_{\text{EE}}^{(r)}$, calculate $y^{(r+1)}$ by

$$y^{(r+1)} = \min_{k \in \mathcal{K}} R_u(1 - \epsilon_u) + R_k(1 - 2\gamma_k \sigma_k^2 / (|g_k^L|^2 \bar{p}_u^{(r+1)} P_U)) - \eta_{\text{EE}}^{(r)} (\bar{p}_b + \bar{p}_u^{(r+1)}) \quad (74)$$

5: Given $y^{(r+1)}$ and $P_u^{(r+1)}$, update $\eta_{\text{EE}}^{(r+1)}$ by

$$\eta_{\text{EE}}^{(r+1)} = \min_{k \in \mathcal{K}} \left\{ R_u(1 - \epsilon_u) + R_k(1 - 2\gamma_k \sigma_k^2 / (|g_k^L|^2 \bar{p}_u^{(r+1)} P_U)) \right\} / (\bar{p}_b + \bar{p}_u^{(r+1)}) \quad (75)$$

6: **until** The convergence criterion $|y^{(r+1)} - y^{(r)}| \leq \Delta_r$ is met or reach the maximum number of iterations r_{max} .

we can resort to the exhaustive search to achieve its optimal solution quickly. Moreover, we can search $\{b_k\}_{k=1}^K$ in parallel.

C. Algorithm Design

Finally, according to the above analysis and derivation, we can summarize the main steps of the joint RIS Phase shift, Transmit Power, and Blocklength optimization (PTPB) algorithm for mitigating the formulated energy efficiency optimization problem in Algorithm 3.

The computational complexity of the proposed algorithm consists of three contributors: 1) *Channel estimation*: R-OAMP includes a module A, a module B, and a parameter updating module. Module A is an LMMSE estimator with a complexity of $O(PN)$. Module B is an MMSE estimator where a sum-product approach is leveraged, which thus has a low computational complexity of $O(N)$. The complexity of updating offsets is $O(PN^2)$. Considering that the above modules should be iteratively executed for no more than I_c^{max} times. The computational complexity of R-OAMP is $O(f_1) = O(I_c^{\text{max}}(PN + N + PN^2))$ in the worst-case. However, empirical evidence shows that R-OAMP usually converges in 30 iterations. 2) *RIS phase shift optimization*: The complexity of solving (57) using an interior-point method dominates the complexity of this contributor and is $O((1 + L)^{3.5})$ [46]. 3) *Joint power and blocklength optimization*: This joint optimization model includes the BS-Layer optimization and the UAV-Layer optimization. As the iterative method in BS-Layer optimization will converge in two iterations, the complexity of BS-Layer optimization is dominated by the exhaustive search approach and is $O(f_2) = O((B_u^{\text{max}} - B_u^{\text{min}})S_1 + \log_2(B_u^{\text{max}} - B_u^{\text{min}}))$, where S_1 is the complexity of computing (67a). For UAV-Layer optimization, it needs to iteratively optimize (69) and (76) for no more than c_{max} iterations. The complexities of optimizing UAV transmit power and blocklength are $O(r_{\text{max}}2^{3.5})$ and $O((B^{\text{max}} - B^{\text{min}})S_2 + \log_2(B^{\text{max}} - B^{\text{min}}))$ per iteration, where S_2 is the complexity of computing (76a). Thus, the complexity of UAV-Layer optimization is $O(f_3) = O(c_{\text{max}}(r_{\text{max}}2^{3.5} + (B^{\text{max}} - B^{\text{min}})S_2 + \log_2(B^{\text{max}} - B^{\text{min}})))$ in the worst-case. Then, the total computational complexity of is $O(f_1 + f_2 + (1 + L)^{3.5} + f_3)$ in the worst-case.

Algorithm 3 Joint RIS Phase shift, Transmit Power, and Blocklength optimization, PTPB

- 1: **Initialization:** Run the initialization steps in R-OAMP and Algorithm 2. Let $c_{\max} = 100$, $r = 0$. $I_{\max} = 10$.
 - 2: **Channel estimation and RIS phase shift optimization:**
 - 3: Call the channel estimation approach (R-OAMP) to estimate the HAP-UAV channel gain \mathbf{h} .
 - 4: Compute \mathbf{v} by (50) and optimize (57) using MOSEK to obtain ω_{l_0} . Compute θ_n by (54).
 - 5: Given the obtained \mathbf{h} , \mathbf{v} , and Θ , compute SNR_u by (3).
 - 6: **BS-Layer optimization:**
 - 7: **repeat**
 - 8: Given $b_u^{(i)}$ compute $P_b(b_u^{(i)})^{(i+1)}$ by (65).
 - 9: Given $P_b(b_u^{(i)})^{(i+1)}$, and any non-zero P_U and $\{b_k\}$, exhaustively search $b_u^{(i+1)}$ such that (67a) is maximized, subject to (67b). Update $i = i + 1$.
 - 10: **until** Converge or reach the maximum number of iterations I_{\max} .
 - 11: **UAV-Layer optimization:**
 - 12: **repeat**
 - 13: Call Algorithm 2 to obtain $P_u^{(c+1)}$.
 - 14: **for** each $k \in \{1, 2, \dots, K\}$ in parallel **do**
 - 15: Given $P_u^{(c+1)}$, solve the following problem using an exhaustive search method

$$\begin{aligned} \max_{b_k} \quad & R_k(1 - \epsilon_k) \\ \text{s.t.} \quad & 2\gamma_k / \overline{SNR_k} \leq \epsilon_k^{\text{th}} \\ & B^{\min} \leq b_k \leq B^{\max}, \quad b_k \in \mathbb{Z}^+ \end{aligned} \tag{77a} \tag{77b} \tag{77c}$$
 - 16: **end for**
 - 17: Update $c = c + 1$.
 - 18: **until** Converge or $c = c_{\max}$.
-

V. SIMULATION RESULTS

A. Comparison Algorithms and Simulation Parameters

In this section, we evaluate the performance of the proposed channel estimation approach, RIS phase shift optimization strategy, and resource optimization algorithm, respectively. For this aim, the following benchmark algorithms are respectively compared: **OMP** [47]: The OMP approach is an improved version of the well-known matching pursuit approach. **SBL** [42]: The sparse Bayesian learning (SBL) approach recovers sparse channel vectors based on a sparse Bayesian learning theory. **SP** [48]: The subspace pursuit (SP) approach identifies the signal support based on the maximum correlation criterion and is robust to measurement noises. **Random-Phase**: In this algorithm, each element of the HAP-RIS is assigned with a random phase shift. **Zero-Phase**: In this algorithm, all elements of the HAP-RIS are assigned with a zero phase shift. **Exhaustive-Phase**: It exhaustively searches for the AoD of the optimal phase alignment path ω_{l_0} in the interval $[0, \pi/2]$. **MTP**: The difference between the maximum transmit

power-based (MTP) algorithm and the proposed algorithm lies in that MTP adopts the maximum BS transmit power and the maximum UAV transmit power. **MBL**: The difference between the maximum blocklength-based (MBL) algorithm and the proposed algorithm lies in that MBL is configured with the maximum BS blocklength and the maximum UAV blocklength.

We consider a square area \mathcal{G} of size $500 \times 500 \text{ m}^2$, the location of the center point of which is $[80 \text{ km}, 0 \text{ km}]$. The robots are randomly distributed in \mathcal{G} . Both path loss of the BS-HAP channel and large-scale channel fading of the HAP-UAV channel are generated by the propagation model in [49]. The HAP-UAV small-scale channel realization consists of $L = 8$ propagation paths to simulate the sparsity characteristic, and AoDs $\{\omega_l\}$ are assumed to follow an i.i.d. uniform distribution in an angular interval of $\pi/12$ centered on the LoS direction between the HAP and the UAV due to the limited scattering environment around the UAV. Considering the requirements of HAP-UAV channel sparsity along with BS-HAP-UAV long-distance propagation, we set the carrier frequency $f_{\text{BS}} = 6 \text{ GHz}$ [21]. As for the UtG channel model, we assume that the channel fading consists of large-scale and small-scale channel fading [50]. We leverage the channel model in [51] and thereof channel parameters of a suburban scenario to calculate the UtG large-scale channel fading. The rayleigh fading model is utilized to model UtG small-scale channel fading². Further, the small-scale fading coefficient is assumed to be an i.i.d. random variable with zero mean and unit variance. The inter-element spacing of the RIS is assumed to be half-wavelength. More system parameters are listed as below: $M = 32$, $N = 128$, $\mathbf{p}_H = [1, 0, 18]^T \text{ km}$, $K = 10$, $\mathbf{p}_U = [80, 0, 0.05]^T \text{ km}$, $F_B = 80 \text{ bits}$, $B_u^{\min} = 100 \text{ bits}$, $B^{\min} = 100 \text{ bits}$, $B_u^{\max} = 1000 \text{ bits}$, $B^{\max} = 1000 \text{ bits}$, $P_B = 120 \text{ W}$, $P_U = 0.5 \text{ W}$, $f_{\text{UAV}} = 2 \text{ GHz}$ [21], $\varepsilon_u^{\text{th}} = 0.00005$, $\varepsilon_k^{\text{th}} = 0.00005$, $G = 4 \text{ dB}$, $\sigma_0^2 = -134 \text{ dBm}$, $\sigma_k^2 = -143 \text{ dBm}$, $\zeta = 0$, $\rho = 1$, $F_k = 80 \text{ bits}$ [31].

B. Performance Evaluation

We design extensive simulations to comprehensively evaluate the performance of the proposed algorithm, particularly including the verification of the accuracy of the proposed channel estimation approach, the effectiveness of the designed RIS phase shift optimization strategy along with the superiority of the proposed resource allocation algorithm. All comparison approaches and algorithms in the simulations are executed 200 times, and the final simulation result is the averaged one.

1) *Results of Channel Estimation*: In this simulation, we compare the proposed R-OAMP approach with other channel estimation approaches, including OMP, SBL, and SP. The parameters $\{\lambda, \varsigma, \rho\}$ are automatically updated by adopting an expectation-maximization algorithm during each iteration [52]. The metric, normalized mean square error (NMSE), is selected to evaluate the performance of channel estimation approaches, which is defined as

$$NMSE(\hat{\mathbf{h}}) \triangleq \|\hat{\mathbf{h}} - \mathbf{h}\|^2 / \|\mathbf{h}\|^2 \quad (78)$$

where $\hat{\mathbf{h}}$ is the estimation of \mathbf{h} .

We plot the tendency of estimation accuracy of all compared channel estimation approaches under different $SNR_u \in \{0, 4, 8, 12, 16, 20\}$, as shown in Fig. 6. From this figure, we can observe that: 1) For all channel

²As the UtG channel is not sparse [50], we cannot leverage the proposed channel estimation approach to estimate its small-scale fading.

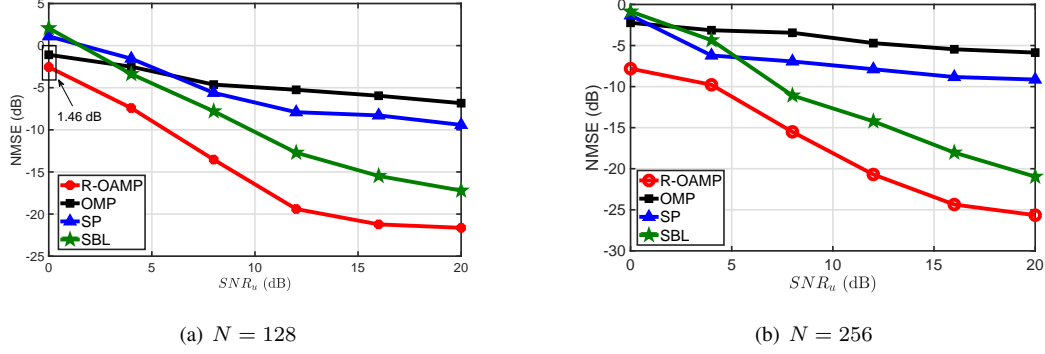


Fig. 6. NMSE versus received SNR of UAV SNR_u , $P = 48$.

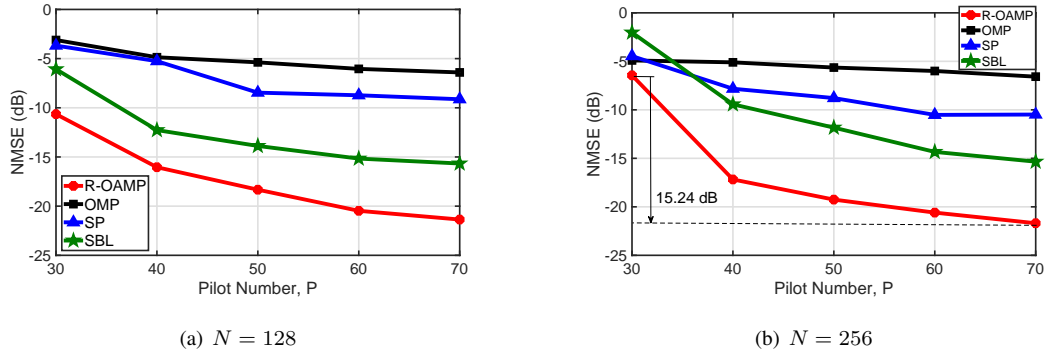


Fig. 7. NMSE versus the number of pilot sequences P , $SNR_u = 15\text{dB}$.

estimation approaches, their estimation performance will be improved with an increasing SNR_u . 2) Compared with other estimation approaches, the estimation accuracy is improved by at least 1.46 dB using R-OAMP. 3) When there are more RIS reflecting elements, which indicates that the HAP-UAV channel becomes sparser, the estimation accuracy of the proposed approach is further improved.

The estimation performance of all compared channel estimation approaches versus the number of pilot sequences P is illustrated in Fig. 7. We can obtain the following observations from this figure: 1) Except for OMP, the obtained NMSE of the rest estimation approaches decreases sharply with an increasing number of pilot sequences. For example, the obtained NMSE by R-OAMP decreases by 15.24 dB when P increases from 30 to 70. 2) R-OAMP can always achieve the smallest NMSE under different P and N . It demonstrates that R-OAMP can achieve more accurate channel estimation results with lower pilot overhead by exploiting the sparsity prior of the HAP-UAV channel in the angular domain.

2) *Results of RIS Phase Shift Optimization:* In this simulation, we compare the proposed algorithm with two benchmarks, i.e., Random-Phase and Zero-Phase, to verify its effectiveness regarding RIS phase shift optimization.

The tendency of the cascaded BS-HAP-UAV channel gain versus the number of RIS passive reflecting elements $N \in \{96, 128, 160, 192, 224, 256\}$ is plotted in Fig. 8. We can observe from this figure that: 1) PTPB outweighs the benchmarks and improves the BS-HAP-UAV channel gain by at least 20.36 dB. 2) PTPB achieves a cascaded

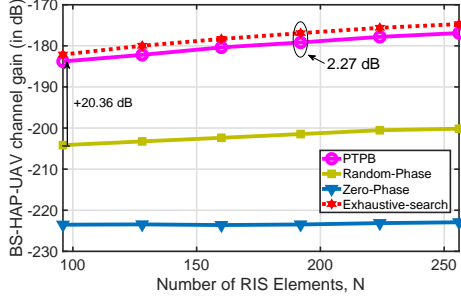


Fig. 8. BS-HAP-UAV channel gain versus the number of RIS elements N .

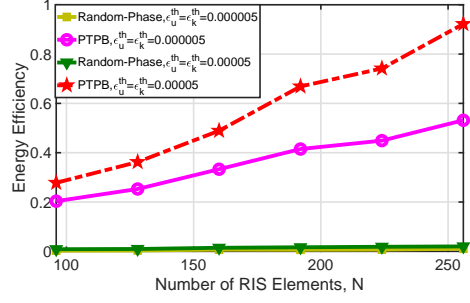


Fig. 9. Achieved energy efficiency versus the number of RIS elements N .

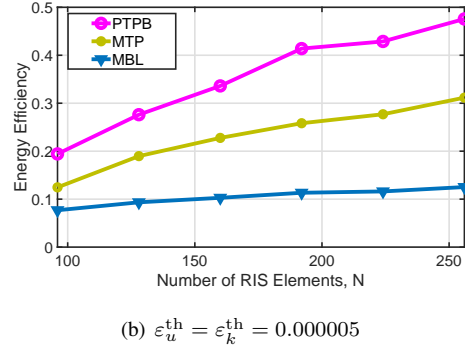
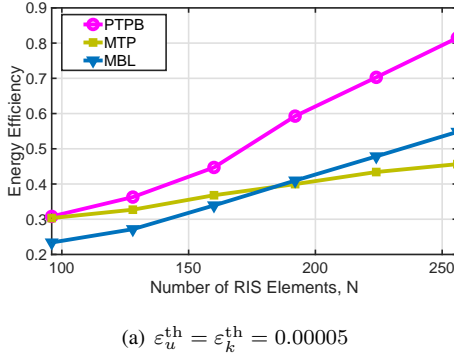


Fig. 10. Achieved energy efficiency versus the number of RIS elements N .

channel gain that is close to the channel gain obtained by the Exhaustive-Phase algorithm, and their difference is less than 3 dB. 3) The obtained channel gain by PTPB monotonically increases with the number of RIS elements, while the benchmarks fail to unlock the significant advantage of RIS in terms of addressing the channel fading issue.

Besides, we adopt the evaluation metric, energy efficiency computed by (20a), to further verify the effectiveness of the designed RIS phase shift optimization strategy. We plot the obtained energy efficiency of the comparison algorithms under different numbers of RIS elements and reliability constraints in Fig. 9. By referring to Fig. 8, the achieved BS-HAP-UAV channel gains by both Random-Phase and Zero-Phase are extremely small. The results in Fig. 9 illustrate that the proposed algorithm can achieve higher energy efficiency and satisfy the reliability requirement with a lower transmit power budget. From the results in Figs. 8 and 9, we can draw the conclusion that PTPB can effectively deal with the phase alignment issue in a RIS-integrated multipath EM propagation environment.

3) Results of Transmit Power and Blocklength Optimization: To verify the effectiveness of the proposed algorithm regarding joint transmit power and blocklength optimization, we compare it with two benchmark algorithms, i.e., MTP and MBL. To this end, we evaluate the impact of the number of the RIS elements N , the side length of \mathcal{G} , and the UAV transmit power budget P_U , respectively.

Fig. 10 shows the achieved energy efficiency of all comparison algorithms over the number of RIS elements. From this figure, we can obtain the following observations: 1) PTPB outperforms the other two benchmarks under

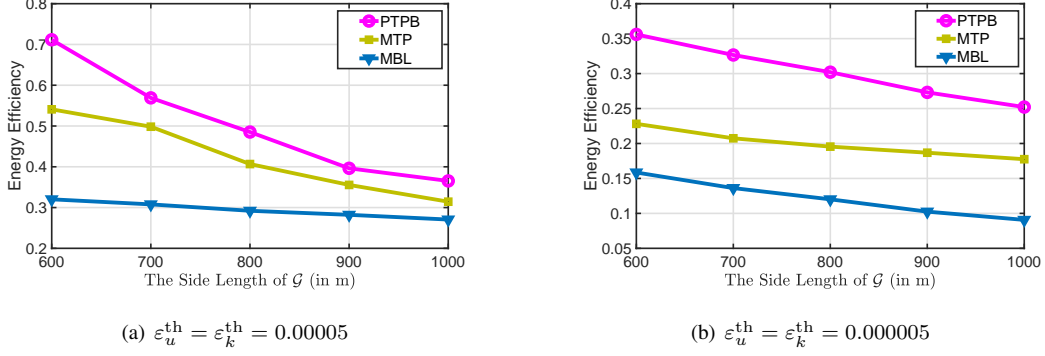


Fig. 11. Achieved energy efficiency versus the side length of \mathcal{G} .

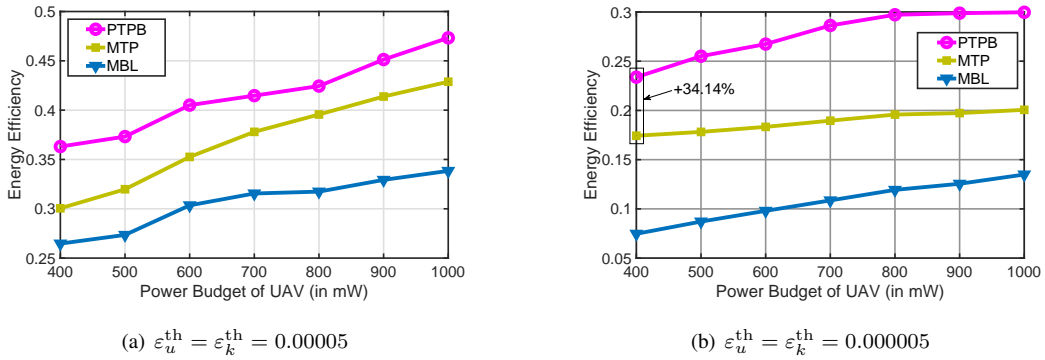


Fig. 12. Achieved energy efficiency versus the transmit power budget of UAV.

diverse N , $\varepsilon_u^{\text{th}}$, and $\varepsilon_k^{\text{th}}$. The achieved energy efficiency by all comparison algorithms increases with an increasing number of RIS elements. This is due to the improvement in the BS-HAP-UAV channel quality, and then fewer resources (including transmit power and blocklength) are required to satisfy URLLC requirements. 2) When a more stringent reliability requirement, i.e., $\varepsilon_u^{\text{th}} = \varepsilon_k^{\text{th}} = 0.000005$, is enforced, the obtained energy efficiency of all comparison algorithms will decrease. Obviously, more resources will be consumed to satisfy the more stringent reliability requirement. 3) Under a more stringent reliability constraint, the energy efficiency obtained by MBL does not increase effectively with improved channel conditions. In this case, the transmit power cannot be significantly reduced owing to the strictly limited blocklength.

Fig. 11 plots the tendency of the obtained energy efficiency of all comparison algorithms versus the side length of the coverage area \mathcal{G} . From this figure, we can observe that: 1) PTPB obtains the maximum energy efficiency under different side lengths of \mathcal{G} . 2) The achieved energy efficiency by PTPB decreases as the area of the coverage area increases. Enlarging the area of the coverage area indicates that more robots will be distributed at the edge of the UAV cell, which thus consumes more resources and decreases the achieved energy efficiency.

Finally, we plot the tendency of the obtained energy efficiency of all comparison algorithms over the transmit power budget of UAV $P_U \in \{400, 500, 600, 700, 800, 900, 1000\}$ mW in Fig. 12. In this simulation, we set the maximum blocklength $B_u^{\text{max}} = B^{\text{max}} = 1000$ bits. The following observations can be obtained from this figure: 1)

PTPB achieves the highest energy efficiency. For instance, under a tighter reliability constraint, the system energy efficiency can be improved by at least 34.14% by executing the proposed PTPB algorithm. 2) The performance of MBL degrades more compared to MTP when a more stringent reliability constraint is imposed. The reasons are as follows: compared to the case of $\varepsilon_u^{\text{th}} = \varepsilon_k^{\text{th}} = 0.00005$, MBL needs to allocate higher transmit power to satisfy the tighter reliability requirement in the case of $\varepsilon_u^{\text{th}} = \varepsilon_k^{\text{th}} = 0.000005$. Owing to the limited feasible region of blocklength and the adoption of the maximum transmit power, the obtained energy efficiency by MTP will not be significantly reduced when a more stringent reliability requirement is imposed.

Summarily, from the above simulation results, we can conclude that joint RIS phase shift, transmit power, and blocklength optimization can significantly improve the system energy efficiency.

VI. CONCLUSION

This paper proposed to deploy a RIS-integrated NSIN to provide energy-efficient URLLC services for remote robots, which leveraged the advantages of RIS and power control. For this aim, we formulated the energy-efficient URLLC service provision problem as a resource optimization problem aiming at maximizing the effective throughput and minimizing the system power consumption, subject to URLLC and physical resource constraints. This problem was difficult to be mitigated due to the unknown channel model and intractable analysis. To handle these challenges, we developed a novel channel estimation approach, derived an analysis-friendly expression of DEP, and decomposed the problem by analyzing its monotonicity. Based on the above results, we proposed a joint RIS phase shift, transmit power, and blocklength optimization algorithm, the computational complexity of which was also analyzed. Simulation results verified that the developed channel estimation approach could accurately estimate HAP-UAV channels and the proposed resource optimization algorithm was more energy-efficient than benchmarks. This paper investigated a stationary scenario, and extending it to a mobility scenario (e.g., the UAV is moving) will be an interesting topic worthy of study in the near future. In this case, channel tracking and RIS phase shift optimization approaches adapted to moving UAVs need to be designed.

APPENDIX

A. Proof of Lemma 1

In practice, we don't know the off-grid offsets in advance. Nevertheless, if we deploy a great number of antenna elements, the measurement matrix $\mathbf{F}(\Delta\phi) \approx \mathbf{F}(\mathbf{0})$. Therefore, without loss of generality, we set the corresponding off-grid offsets to zero when generating the pilot matrix. Particularly, we then have

$$\mathbf{F}(\Delta\phi) \approx \mathbf{F}(\mathbf{0}) = \mathbf{S}\mathbf{D}\mathbf{R} \quad (79)$$

where $\mathbf{S} = \{0, 1\}^{P \times N}$ is a selection matrix generated by randomly selecting and reordering P rows of an $N \times N$ identity matrix, $\mathbf{D} \in \mathbb{C}^{N \times N}$ is the DFT matrix, $\mathbf{R} \in \mathbb{C}^{N \times N}$ is a random permutation matrix generated by randomly reordering an $N \times N$ identity matrix. Note that the measurement matrix comprises the pilot matrix, BS-HAP channel matrix, and RIS phase shift matrix. We can compute the channel state information (CSI) of the BS-HAP channel in

advance and can impose $\theta_n = -2\pi(n-1)\bar{d}_{\text{RIS}}(\sin(\arctan(\frac{\|[\mathbf{x}_H, \mathbf{y}_H]^T - [\mathbf{x}_U, \mathbf{y}_U]^T\|_2}{|h_H - h_U|})) - \sin(v_{\text{AoA}}))$, $\forall n$, in the stage of designing the pilot matrix. Then, the pilot matrix to be transmitted by the BS can be expressed as

$$\mathbf{U}_0^H = \mathbf{S} \mathbf{D} \mathbf{R} (\bar{\mathbf{H}}^H \boldsymbol{\Theta}^H \mathbf{A}(0))^{-1} \quad (80)$$

B. Off-Grid Offsets Update

Given the estimated $\hat{p}(\mathbf{x}) = \mathcal{CN}(0; \mathbf{x}_B^{\text{post}}, v_B^{\text{post}} \mathbf{I})$ at the i -th iteration, the progressively refined function in (47) can be computed by

$$\begin{aligned} \hat{r}(\Delta\phi; \Delta\phi^i) &\propto \mathbb{E}_{\hat{p}(\mathbf{x}|\mathbf{y}, \Delta\phi)} [-\frac{1}{\sigma_e^2} \|\mathbf{y} - \mathbf{F}(\Delta\phi)\mathbf{x}\|^2] \\ &\propto -\frac{1}{\sigma_e^2} (\|\mathbf{y} - \mathbf{F}(\Delta\phi)\mathbf{x}_B^{\text{post}}\|^2 + v_B^{\text{post}} \text{tr}(\mathbf{F}(\Delta\phi) \mathbf{F}(\Delta\phi)^H)) \end{aligned} \quad (81)$$

The derivative of $\hat{r}(\Delta\phi; \Delta\phi^i)$ in (83) can be calculated as $\boldsymbol{\psi}_{\Delta\phi}^{(i)} = [\psi^{(i)}(\Delta\phi_1), \dots, \psi^{(i)}(\Delta\phi_N)]^T$, where

$$\begin{aligned} \psi^{(i)}(\Delta\phi_n) &= 2\text{Re}(\mathbf{a}'(\hat{\omega}_n + \Delta\phi_n)^H \mathbf{U}_0 \bar{\mathbf{H}} \boldsymbol{\Theta} (\mathbf{U}_0 \bar{\mathbf{H}} \boldsymbol{\Theta})^H \mathbf{a}(\hat{\omega}_n + \Delta\phi_n)) \\ &\times \varphi_1^{(i)} + 2\text{Re}(\mathbf{a}'(\hat{\omega}_j + \Delta\phi_j)^H \mathbf{U}_0 \bar{\mathbf{H}} \boldsymbol{\Theta} \varphi_2^{(i)}) \end{aligned} \quad (82)$$

with $\varphi_1^{(i)} = -\frac{1}{\sigma_e^2} (|\mathbf{x}_{B,n}^{\text{post}}|^2 + v_B^{\text{post}})$, $\varphi_2^{(i)} = \frac{1}{\sigma_e^2} (\mathbf{x}_{B,n}^{\text{post}})^* \mathbf{y}_{-n}$, $\mathbf{y}_{-n} = \mathbf{y} - (\mathbf{U}_0 \bar{\mathbf{H}} \boldsymbol{\Theta})^H \sum_{j \neq n} \mathbf{a}(\hat{\omega}_j + \Delta\phi_j) \mathbf{x}_{B,j}^{\text{post}}$, $\mathbf{a}'(\hat{\omega}_n + \Delta\phi_n) = d\mathbf{a}(\hat{\omega}_n + \Delta\phi_n)/d\Delta\phi_n$.

Then we can update the off-grid offsets as

$$\Delta\phi^{i+1} = \Delta\phi^i + \alpha_i \boldsymbol{\psi}_{\Delta\phi}^{(i)} \quad (83)$$

C. Proof of Lemma 2

Define the matrix $\boldsymbol{\Lambda} = \mathbf{h}^H \boldsymbol{\Theta} \mathbf{H}$. Then, we can rewrite SNR_u in (3) as

$$\text{SNR}_u = P_b G \mathbf{v}^H \boldsymbol{\Lambda}^H \boldsymbol{\Lambda} \mathbf{v} / \sigma_0^2 \quad (84)$$

According to (6) and (9), $\boldsymbol{\Lambda}^H \boldsymbol{\Lambda}$ is a rank-1 matrix with the following structure

$$\boldsymbol{\Lambda}^H \boldsymbol{\Lambda} = D \mathbf{a}_{\text{BS}}(v_{\text{AoD}}) \mathbf{a}_{\text{BS}}(v_{\text{AoD}})^H \quad (85)$$

where D is a positive constant.

The non-zero eigenpair of $\boldsymbol{\Lambda}^H \boldsymbol{\Lambda}$ can then be expressed as

$$(E_{\text{val}}, E_{\text{vec}}) = (D \|\mathbf{a}_{\text{BS}}(v_{\text{AoD}})\|_2^2, \frac{\mathbf{a}_{\text{BS}}(v_{\text{AoD}})}{\|\mathbf{a}_{\text{BS}}(v_{\text{AoD}})\|_2}) \quad (86)$$

Owing to the unit magnitude of \mathbf{v} and the Rayleigh-Ritz theorem, \mathbf{v} can be calculated by

$$\mathbf{v} = \frac{\mathbf{a}_{\text{BS}}(v_{\text{AoD}})}{\|\mathbf{a}_{\text{BS}}(v_{\text{AoD}})\|_2} \quad (87)$$

D. Proof of Lemma 3

Define \mathcal{P} as the feasible region of (69), and $\eta_{EE} = \min_{k \in \mathcal{K}} \frac{R_u(1 - \epsilon_u) + R_k(1 - \epsilon_k)}{\bar{p}_b + \bar{p}_u} = \min_{k \in \mathcal{K}} \frac{V_k(\bar{p}_u)}{S(\bar{p}_u)}$. Denote by η_{EE}^* and $(\bar{p}_u^* P_U) \in \mathcal{P}$ the optimal energy efficiency and the optimal UAV transmit power, respectively. Then, we have

$$\eta_{EE}^* = \frac{\min_{k \in \mathcal{K}} V_k(\bar{p}_u^*)}{S(\bar{p}_u^*)} \geq \frac{\min_{k \in \mathcal{K}} V_k(\bar{p}_u)}{S(\bar{p}_u)} \quad (88)$$

Accordingly, the following equation holds

$$\max_{P_u} \min_{k \in \mathcal{K}} V_k(\bar{p}_u) - \eta_{EE}^* S(\bar{p}_u) = 0 \quad (89)$$

On the contrary, suppose that $(\bar{p}_u^* P_U)$ is the optimal UAV transmit power of the following optimization problem

$$\max_{P'_u} \min_{k \in \mathcal{K}} V_k(P'_u/P_U) - \eta_{EE}^* S(P'_u/P_U) \quad (90a)$$

$$\text{s.t : Constraints (18), (20c).} \quad (90b)$$

and the following equation holds

$$\min_{k \in \mathcal{K}} V_k(\bar{p}_u^*) - \eta_{EE}^* S(\bar{p}_u^*) = 0 \quad (91)$$

As (69) and (90) have the same feasible region \mathcal{P} , for any UAV transmit power $P'_u \in \mathcal{P}$, the following inequality holds

$$\min_{k \in \mathcal{K}} V_k(P'_u/P_U) - \eta_{EE}^* S(P'_u/P_U) \leq \min_{k \in \mathcal{K}} V_k(\bar{p}_u^*) - \eta_{EE}^* S(\bar{p}_u^*) = 0 \quad (92)$$

From (92), we obtain $\eta_{EE}^* = \frac{\min_{k \in \mathcal{K}} V_k(\bar{p}_u^*)}{S(\bar{p}_u^*)} \geq \frac{\min_{k \in \mathcal{K}} V_k(P'_u/P_U)}{S(P'_u/P_U)}$. Then we can conclude that (69) and (90) have the same optimal UAV transmit power. This completes the proof.

REFERENCES

- [1] A. Brighente, J. Mohammadi, P. Baracca, S. Mandelli, and S. Tomasin, "Interference prediction for low-complexity link adaptation in beyond 5g ultra-reliable low-latency communications," *IEEE Trans. Wirel. Commun.*, vol. 21, no. 10, pp. 8403–8415, 2022.
- [2] G. K. Kurt, M. G. Khoshkholgh, S. Alfattani, A. Ibrahim, T. S. J. Darwish, M. S. Alam, H. Yanikomeroglu, and A. Yongaçoglu, "A vision and framework for the high altitude platform station (HAPS) networks of the future," *IEEE Commun. Surv. Tutorials*, vol. 23, no. 2, pp. 729–779, 2021.
- [3] D. Wang, S. A. Al-Ahmed, and M. Z. Shakir, "Optimized link distribution schemes for ultrareliable and low-latent communications in multilayer airborne networks," *IEEE Trans. Ind. Informatics*, vol. 16, no. 9, pp. 5866–5873, 2020.
- [4] MST-PRC. Comprehensive security technology for railway transportation operation and safety based on air-space-vehicle-ground information collaboration. Feb. 13, 2019. [Online]. Available: https://www.most.gov.cn/ztzl/lhzt/lhzt2019/jjkjlhzt2019/201902/t20190227_145277.html
- [5] N. S. Perovic, L. Tran, M. D. Renzo, and M. F. Flanagan, "Achievable rate optimization for MIMO systems with reconfigurable intelligent surfaces," *IEEE Trans. Wirel. Commun.*, vol. 20, no. 6, pp. 3865–3882, 2021.
- [6] A. Ranjha, G. Kaddoum, and K. Dev, "Facilitating URLLC in UAV-assisted relay systems with multiple-mobile robots for 6G networks: A prospective of agriculture 4.0," *IEEE Trans. Ind. Informatics*, vol. 18, no. 7, pp. 4954–4965, 2022.
- [7] C. M. W. Basnayaka, D. N. K. Jayakody, and Z. Chang, "Age-of-information-based URLLC-enabled UAV wireless communications system," *IEEE Internet Things J.*, vol. 9, no. 12, pp. 10212–10223, 2022.
- [8] G. Bartoli and D. Marabissi, "CQI prediction through recurrent neural network for UAV control information exchange under URLLC regime," *IEEE Trans. Veh. Technol.*, vol. 71, no. 5, pp. 5101–5110, 2022.

- [9] K. Wang, C. Pan, H. Ren, W. Xu, L. Zhang, and A. Nallanathan, "Packet error probability and effective throughput for ultra-reliable and low-latency UAV communications," *IEEE Trans. Commun.*, vol. 69, no. 1, pp. 73–84, 2021.
- [10] C. She, C. Liu, T. Q. S. Quek, C. Yang, and Y. Li, "Uav-assisted uplink transmission for ultra-reliable and low-latency communications," in *ICC Workshops*. IEEE, 2018, pp. 1–6.
- [11] P. Yang, X. Xi, K. Guo, T. Q. S. Quek, J. Chen, and X. Cao, "Proactive UAV network slicing for URLLC and mobile broadband service multiplexing," *IEEE J. Sel. Areas Commun.*, vol. 39, no. 10, pp. 3225–3244, 2021.
- [12] A. Ranjha and G. Kaddoum, "Quasi-optimization of uplink power for enabling green URLLC in mobile UAV-assisted IoT networks: A perturbation-based approach," *IEEE Internet Things J.*, vol. 8, no. 3, pp. 1674–1686, 2021.
- [13] K. Chen, Y. Wang, J. Zhao, X. Wang, and Z. Fei, "URLLC-oriented joint power control and resource allocation in UAV-assisted networks," *IEEE Internet Things J.*, vol. 8, no. 12, pp. 10 103–10 116, 2021.
- [14] X. Xi, X. Cao, P. Yang, J. Chen, T. Q. S. Quek, and D. Wu, "Network resource allocation for eMBB payload and URLLC control information communication multiplexing in a multi-uav relay network," *IEEE Trans. Commun.*, vol. 69, no. 3, pp. 1802–1817, 2021.
- [15] P. Yang, X. Xi, T. Q. S. Quek, J. Chen, and X. Cao, "Power control for a URLLC-enabled UAV system incorporated with DNN-based channel estimation," *IEEE Wirel. Commun. Lett.*, vol. 10, no. 5, pp. 1018–1022, 2021.
- [16] C. Huang, G. C. Alexandropoulos, A. Zappone, M. Debbah, and C. Yuen, "Energy efficient multi-user MISO communication using low resolution large intelligent surfaces," in *GLOBECOM Workshops*. IEEE, 2018, pp. 1–6.
- [17] Y. Li, C. Yin, T. Do-Duy, A. Masaracchia, and T. Q. Duong, "Aerial reconfigurable intelligent surface-enabled URLLC UAV systems," *IEEE Access*, vol. 9, pp. 140 248–140 257, 2021.
- [18] A. Ranjha and G. Kaddoum, "URLLC facilitated by mobile UAV relay and RIS: A joint design of passive beamforming, blocklength, and UAV positioning," *IEEE Internet Things J.*, vol. 8, no. 6, pp. 4618–4627, 2021.
- [19] X. Zhang, J. Wang, and H. V. Poor, "Statistical QoS-driven beamforming and trajectory optimizations in UAV/IRS-based 6G wireless networks in the non-asymptotic regime," in *ISIT*. IEEE, 2022, pp. 3333–3338.
- [20] M. Samir, M. K. Elhattab, C. Assi, S. Sharafeddine, and A. Ghayeb, "Optimizing age of information through aerial reconfigurable intelligent surfaces: A deep reinforcement learning approach," *IEEE Trans. Veh. Technol.*, vol. 70, no. 4, pp. 3978–3983, 2021.
- [21] H. Jeon, S. Park, J. Park, K. Huang, and C. Chae, "An energy-efficient aerial backhaul system with reconfigurable intelligent surface," *IEEE Trans. Wirel. Commun.*, vol. 21, no. 8, pp. 6478–6494, 2022.
- [22] N. Gao, S. Jin, X. Li, and M. Matthaiou, "Aerial RIS-assisted high altitude platform communications," *IEEE Wirel. Commun. Lett.*, vol. 10, no. 10, pp. 2096–2100, 2021.
- [23] A. Khalili, E. M. Monfared, S. Zargari, M. R. Javan, N. M. Yamchi, and E. A. Jorswieck, "Resource management for transmit power minimization in UAV-assisted RIS HetNets supported by dual connectivity," *IEEE Trans. Wirel. Commun.*, vol. 21, no. 3, pp. 1806–1822, 2022.
- [24] X. Hu, R. Zhang, and C. Zhong, "Semi-passive elements assisted channel estimation for intelligent reflecting surface-aided communications," *IEEE Trans. Wirel. Commun.*, vol. 21, no. 2, pp. 1132–1142, 2022.
- [25] S. Li, B. Duo, M. D. Renzo, M. Tao, and X. Yuan, "Robust secure UAV communications with the aid of reconfigurable intelligent surfaces," *IEEE Trans. Wirel. Commun.*, vol. 20, no. 10, pp. 6402–6417, 2021.
- [26] D. Grace and M. Mohorcic, *Broadband communications via high altitude platforms*. John Wiley & Sons, 2011.
- [27] D. Tse and P. Viswanath, *Fundamentals of Wireless Communication*. Cambridge University Press, 2005.
- [28] Y. Polyanskiy, H. V. Poor, and S. Verdú, "Channel coding rate in the finite blocklength regime," *IEEE Trans. Inf. Theory*, vol. 56, no. 5, pp. 2307–2359, 2010.
- [29] W. Yang, G. Durisi, T. Koch, and Y. Polyanskiy, "Quasi-static multiple-antenna fading channels at finite blocklength," *IEEE Transactions on Information Theory*, vol. 60, no. 7, pp. 4232–4265, 2014.
- [30] L. Yuan, N. Yang, F. Fang, and Z. Ding, "Performance analysis of UAV-assisted short-packet cooperative communications," *IEEE Trans. Veh. Technol.*, vol. 71, no. 4, pp. 4471–4476, 2022.
- [31] C. Pan, H. Ren, Y. Deng, M. El Kashlan, and A. Nallanathan, "Joint blocklength and location optimization for URLLC-enabled UAV relay systems," *IEEE Commun. Lett.*, vol. 23, no. 3, pp. 498–501, 2019.
- [32] J. Cheng, C. Shen, Z. Chen, and N. Pappas, "Robust beamforming design for IRS-aided URLLC in D2D networks," *IEEE Trans. Commun.*, vol. 70, no. 9, pp. 6035–6049, 2022.
- [33] R. Hashemi, S. Ali, N. H. Mahmood, and M. Latva-aho, "Joint sum rate and blocklength optimization in RIS-aided short packet URLLC systems," *IEEE Commun. Lett.*, vol. 26, no. 8, pp. 1838–1842, 2022.

- [34] W. Chang, Z. Meng, K. Liu, and L. Wang, "Energy-efficient sleep strategy for the UBS-assisted small-cell network," *IEEE Trans. Veh. Technol.*, vol. 70, no. 5, pp. 5178–5183, 2021.
- [35] Z. Wang, R. Liu, Q. Liu, J. S. Thompson, and M. Kadoch, "Energy-efficient data collection and device positioning in UAV-assisted IoT," *IEEE Internet Things J.*, vol. 7, no. 2, pp. 1122–1139, 2020.
- [36] J. Chakareski, S. Naqvi, N. Mastronarde, J. Xu, F. Afghah, and A. Razi, "An energy efficient framework for UAV-assisted millimeter wave 5G heterogeneous cellular networks," *IEEE Trans. Green Commun. Netw.*, vol. 3, no. 1, pp. 37–44, 2019.
- [37] K. Ardah, S. Gherekhloo, A. L. F. de Almeida, and M. Haardt, "TRICE: A channel estimation framework for RIS-aided millimeter-wave MIMO systems," *IEEE Signal Process. Lett.*, vol. 28, pp. 513–517, 2021.
- [38] P. Wang, J. Fang, H. Duan, and H. Li, "Compressed channel estimation for intelligent reflecting surface-assisted millimeter wave systems," *IEEE Signal Process. Lett.*, vol. 27, pp. 905–909, 2020.
- [39] A. Taha, M. Alrabeiah, and A. Alkhateeb, "Enabling large intelligent surfaces with compressive sensing and deep learning," *IEEE Access*, vol. 9, pp. 44 304–44 321, 2021.
- [40] S. M. Kay, *Fundamentals of statistical signal processing: estimation theory*. Prentice-Hall, Inc., 1993.
- [41] J. Ma and L. Ping, "Orthogonal AMP," *IEEE Access*, vol. 5, pp. 2020–2033, 2017.
- [42] J. Dai, A. Liu, and V. K. N. Lau, "FDD massive MIMO channel estimation with arbitrary 2D-array geometry," *IEEE Trans. Signal Process.*, vol. 66, no. 10, pp. 2584–2599, 2018.
- [43] C. J. Wu, "On the convergence properties of the EM algorithm," *The Annals of statistics*, pp. 95–103, 1983.
- [44] S. Dhok, P. Raut, P. K. Sharma, K. Singh, and C. Li, "Non-linear energy harvesting in RIS-assisted URLLC networks for industry automation," *IEEE Trans. Commun.*, vol. 69, no. 11, pp. 7761–7774, 2021.
- [45] Y. Gu, H. Chen, Y. Li, and B. Vucetic, "Ultra-reliable short-packet communications: Half-duplex or full-duplex relaying?" *IEEE Wirel. Commun. Lett.*, vol. 7, no. 3, pp. 348–351, 2018.
- [46] Y. Ye, *Interior point algorithms - theory and analysis*, ser. Wiley-Interscience series in discrete mathematics and optimization. Wiley, 1998.
- [47] G. Z. Karabulut and A. Yongacoglu, "Sparse channel estimation using orthogonal matching pursuit algorithm," in *IEEE 60th Vehicular Technology Conference, 2004. VTC2004-Fall. 2004*, vol. 6. IEEE, 2004, pp. 3880–3884.
- [48] W. Dai and O. Milenkovic, "Subspace pursuit for compressive sensing signal reconstruction," *IEEE Trans. Inf. Theory*, vol. 55, no. 5, pp. 2230–2249, 2009.
- [49] A. Alsharoa and M. Alouini, "Improvement of the global connectivity using integrated satellite-airborne-terrestrial networks with resource optimization," *IEEE Trans. Wirel. Commun.*, vol. 19, no. 8, pp. 5088–5100, 2020.
- [50] A. A. Khuwaja, Y. Chen, N. Zhao, M. Alouini, and P. Dobbins, "A survey of channel modeling for UAV communications," *IEEE Commun. Surv. Tutorials*, vol. 20, no. 4, pp. 2804–2821, 2018.
- [51] A. Al-Hourani, K. Sithamparanathan, and S. Lardner, "Optimal LAP altitude for maximum coverage," *IEEE Wirel. Commun. Lett.*, vol. 3, no. 6, pp. 569–572, 2014.
- [52] J. Ziniel and P. Schniter, "Dynamic compressive sensing of time-varying signals via approximate message passing," *IEEE Trans. Signal Process.*, vol. 61, no. 21, pp. 5270–5284, 2013.